2014

Testing a model of alluvial deposition in the Middle Son Valley, Madhya Pradesh, India - IRSL dating of terraced alluvial sediments and implications for archaeological surveys and palaeoclimatic reconstructions

Christina M. Neudorf
University of Wollongong, cmn821@uow.edu.au

Richard G. Roberts
University of Wollongong, rgrob@uow.edu.au

Zenobia Jacobs
University of Wollongong, zenobia@uow.edu.au

Publication Details

Neudorf, C. M., Roberts, R. G. & Jacobs, Z. (2014). Testing a model of alluvial deposition in the Middle Son Valley, Madhya Pradesh, India - IRSL dating of terraced alluvial sediments and implications for archaeological surveys and palaeoclimatic reconstructions. Quaternary Science Reviews, 89 56-69.

Testing a model of alluvial deposition in the Middle Son Valley, Madhya Pradesh, India - IRSL dating of terraced alluvial sediments and implications for archaeological surveys and palaeoclimatic reconstructions

Abstract

Over the past three decades, the Middle Son Valley, Madhya Pradesh, India has been the focus of archaeological, geological, and palaeoenvironmental investigations that aim to reconstruct regional climate changes in the Late Pleistocene and to understand the effects of the ~74 ka Toba super-eruption on ecosystems and human populations in northern India. The most recently published model of alluvial deposition for the Middle Son Valley subdivides its alluvium into five stratigraphic formations, each associated with a specific artefact assemblage. In this study, new cross-valley topographic profiles, field observations and infrared stimulated luminescence (IRSL) age estimates are used to refine this model south of the Rehi-Son River confluence. These data not only provide insights into the fluvial history of the Son River and its response to changes in palaeoclimate, but will also inform future archaeological surveys by constraining the geomorphic context of surficial and excavated artefacts in the area.

Keywords

Middle Son Valley, Alluvial stratigraphy, Indian archaeology, IRSL dating, Potassium feldspar, CAS

Disciplines

Medicine and Health Sciences | Social and Behavioral Sciences

Publication Details

Neudorf, C. M., Roberts, R. G. & Jacobs, Z. (2014). Testing a model of alluvial deposition in the Middle Son Valley, Madhya Pradesh, India - IRSL dating of terraced alluvial sediments and implications for archaeological surveys and palaeoclimatic reconstructions. Quaternary Science Reviews, 89 56-69.

Testing a model of alluvial deposition in the Middle Son Valley, Madhya Pradesh, India — IRSL dating of terraced alluvial sediments and implications for archaeological surveys and palaeoclimatic reconstructions

C. M. Neudorf [a] *, R. G. Roberts [a], Z. Jacobs [a]

[a] Centre for Archaeological Science, School of Earth and Environmental Sciences, University of Wollongong, Wollongong, NSW 2522, Australia

*E-mail of corresponding author: Christina.Neudorf@ufv.ca (Christina M. Neudorf)

*Present address of corresponding author: Dept. of Geography, University of the Fraser Valley, 33844 King Road, Abbotsford, British Columbia, Canada, V2S 7M8

*Phone number of corresponding author: 1-604-557-8982

Abstract

Over the past three decades, the Middle Son Valley, Madhya Pradesh, India has been the focus of archaeological, geological, and palaeoenvironmental investigations that aim to reconstruct regional climate changes in the Late Pleistocene and to understand the effects of the ~74 ka Toba super-eruption on ecosystems and human populations in northern India. The most recently published model of alluvial deposition for the Middle Son Valley subdivides its alluvium into five stratigraphic formations, each associated with a specific artefact assemblage. In this study, new cross-valley topographic profiles, field observations and infrared stimulated luminescence (IRSL) age estimates are used to refine this model south of the Rehi–Son River confluence. These data not only provide insights into the fluvial history of the Son River and its response to changes in palaeoclimate, but will also inform future archaeological surveys by constraining the geomorphic context of surficial and excavated artefacts in the area.

Keywords: Middle Son Valley, alluvial stratigraphy, Indian archaeology, IRSL dating, potassium feldspar

1. Introduction

Terraced alluvial deposits in the Middle Son Valley (MSV), Madhya Pradesh, India contain volcanic ash (Youngest Toba Tuff, YTT) erupted by the Toba super-eruption ~74 ka ago (Storey et al.,

2012) and a rich archaeological record in the form of Palaeolithic, Mesolithic and Neolithic artefacts (Sharma and Clark, 1983) (Fig. 1A). Since the early 1980s, it has been the focus of archaeological, geological, and palaeoenvironmental investigations aimed at reconstructing regional climate changes in the Late Pleistocene and to understand the effects of the Toba volcanic eruption on ecosystems and human populations in northern India (Sharma and Clark, 1983; Jones and Pal, 2009; Williams et al., 2009; Jones, 2010).

Alluvial terraces, ranging from ~5 m to ~35 m above river level (Fig. 1B), have been observed to extend over 70 km along the length of the Son River, between Baghor in the east and Chorhat in the west (Williams and Royce, 1983). These terraces are thought to have formed during a period of tectonic stability, when changes in river sedimentation reflected changes in local plant cover and load-to-discharge ratios in the Son River, which were influenced, in turn, by regional climate (Williams and Royce, 1982; Williams et al., 2006). Proposed models of alluvial deposition for the MSV subdivide its alluvium into five stratigraphic formations that represent specific time periods in its geological and archaeological history (Williams and Royce, 1982, 1983; Williams et al., 2006), including a major phase of prolonged aggradation that is thought to have occurred between ~39 ka and ~16 ka ago (Table 1, Fig. 2). However, the history of alluvial sedimentation is constrained by few numerical ages spread over a wide geographic area (Fig. 1A, Table 2) and the sample site locations and sedimentary contexts for some of these ages are poorly documented (Jones and Pal, 2009) (Table 2). In the absence of reliable numerical ages, the chronology of human occupation in the MSV has been based on qualitative correlations between artefacts and sediments presumed to be part of one or more of these formations (Williams and Royce, 1982; Sharma and Clark, 1983; Haslam et al., 2012).

According to a recently proposed geomorphic model based on a series of numerical ages from both the Son and Belan Valleys (Williams et al., 2006), the highest alluvial terraces on either side of the Son River (~30–35 m above river level) record the end of a period of aggradation ~16 ka ago coinciding with the termination of deposition of the fine member of the Baghor Formation (Fig. 2). (In this paper, river level refers to the low-stage level of the river as measured during the winter season.) These terraces, 2 as well as the ~10 m-high terraces comprising the Khetaunhi Formation, are considered depositional features in the landscape (Fig. 2) (Williams et al., 2006). Terraces at ~25 m and ~15 m above river level are considered to be erosional features that expose Patpara Formation sediments (Fig. 2) (Williams et al., 2006). In this study, the accuracy of this model is tested near the Rehi–Son confluence using satellite imagery of the area, field observations, cross-valley topographic profiles and infrared stimulated luminescence (IRSL) ages for terraced alluvial sediments. These data provide insights into the fluvial history of the Son River and its response to changes in palaeoclimate, and will inform future archaeological surveys by constraining the geomorphic context of surficial and excavated artefacts in the area.

1.2 Study area and climate

The reach of the Son River examined near the Rehi–Son confluence is shown in Figures 3B and 3C. North of the river, the topography is variable where gullies and streams have incised non-cohesive alluvial silts and sands. In the northwest, NE–SW trending bedrock ridges composed of sandstones and shales outcrop along the north bank of the river and ~1 km further north. Archaeological excavations at the site of Dhaba (Haslam et al., 2012) were conducted in March, 2009. One trench (site 3) was dug in colluvial sediments on the easternmost flanks of the bedrock ridge, and two trenches (sites 1 and 2) were dug in floodplain silts and sands overlying quartzite and shale bedrock on the north bank of the Son River, closer to the Rehi–Son confluence (Figs. 1B, 3C). These excavations have yielded Acheulean, Middle Palaeolithic and microlithic artefacts (Haslam et al., 2012), for which unpublished IRSL ages of about 24–80 ka have been obtained, together with an undated Late Acheulean quarry. East of the Rehi–Son confluence is the Ghoghara main section, which exposes reworked and in situ remnants of YTT (Williams et al., 2009; Gatti et al., 2011; Smith et al., 2011). A prominent east–west trending terrace escarpment lies ~500–700 m south of the Son River channel, and, north of this, gently undulating 5
topography slopes toward the river (Figs. 3B, 3C). A slight break in the topography trends east–west, 6

subparallel to the dirt road (Fig. 3C, and observed during field surveys on foot); this may mark the edge of another alluvial terrace.

The climate of the MSV is influenced by the Southern Oscillation, the NE (winter) monsoon, and to a large extent, the SW (summer) monsoon (Prasad and Enzel, 2006; Williams et al., 2006). In the summer months of June to September, the Intertropical Convergence Zone migrates northwards and the surface winds associated with the SW monsoon bring large amounts of precipitation to the Indian subcontinent. During the winter, northeasterly surface winds bring cold, dry continental air. The precipitation associated with the SW monsoon drives river discharge and can substantially influence river flow dynamics, sedimentation and morphology (Srivastava et al., 2001; Williams et al., 2006; Gibling et al., 2008; Roy et al., 2012). Palaeoclimate data and climate model simulations suggest that two mechanisms exert the dominant forcing on millennial-scale variations in SW monsoon strength. These are changes in the orbit of the Earth, predominantly in the precession of the equinoxes (which control the amount of insolation reaching the Earth as a function of season and, hence, the ability of the Tibetan Plateau to warm in the summer) and changes in glacial boundary conditions (i.e., ice volume, sea surface temperature, albedo, and atmospheric trace-gas concentrations), which alter the way in which the monsoon reacts to astronomical forcing. Clemens and Prell (1991) and Clemens et al. (1991) have argued that while precession-forced insolation changes are the major pacemaker of monsoon strength, glacial boundary conditions have played a relatively minor role in determining the timing and strength of the SW monsoon.

2. Methods

2.1 Topographic surveys

Topographic profiles were measured across the valley along two traverses (A–A' and B–B') near the Rehi–Son confluence (Fig. 3C) using a differential global positioning system (DGPS) and electronic total station (ETS). Control points were measured in open (treeless) spaces near each planned traverse using a Trimble R3 Differential DGPS consisting of one reference receiver and 2 rovers. These control points served as benchmarks to which the start and end points of each traverse (measured using the ETS) were tied. The latitude and longitude coordinates for the start and end points for traverse A–A’ are 24°29.93’N, 82°0.38’E and 24°29.92’N, 82°0.41’E, respectively and those for traverse B–B’ are 24°30.12’N, 82°0.97’E and 24°30.13’N, 82°1.05’E. Control points were logged in static mode for 1.5 h using horizontal baseline lengths of ~100–150 m to achieve measurement precisions better than 0.01 m, and the DGPS data were processed using Trimble Geomatics Office software. A Pentax 326EX ETS was used to measure elevations at 5 m intervals along each traverse. The estimated mean error for each elevation measurement is less than 4 mm. The ETS data were imported into an ArcGIS workspace, and superimposed on georeferenced WorldView-1 panchromatic satellite imagery (50 cm horizontal resolution) of the study area (Fig. 3C).

2.2 IRSL sample collection and measurements

Two samples, GHO-3 and GHO-2 (Neudorf et al., 2012, submitted), were collected from above and below YTT ash, respectively, at the Ghoghara main section (Figs. 3 and 4, Table 3). This section exposes ~11 m (vertical thickness) of generally fining-upward fluvial gravels, sands and silts, with YTT ash appearing between 6 and 7 m below the ground surface. The ground surface is estimated to be within ~5–10 m of the maximum height of the MSV alluvium in this reach of the Son River, as the top-most sands and silts have been eroded away. In addition, seven samples for IRSL dating were collected from alluvial sediments on the south side of the Son River (see Supplementary Table 1 for sample site coordinates): two samples (H-1 and H-5) were collected from near the top of the highest terrace, three samples (M-2, M-4 and M-6) from exposed sediments or roadcuts along the dirt road, and two samples (L-3 and L-7) from gully exposures in the lowest alluvial terrace, next to the river channel (Fig. 3C). The sediments at each sample location were photographed and their texture, colour and sedimentary structures were recorded. Steel tubes, ~5 cm in diameter, were hammered into the face of the exposed sediments. On the south side of the river, samples were taken ~60 to ~100 cm below the ground surface to avoid sampling sediments disturbed by local farming practices (i.e., ploughing). After the tubes had been extracted, the sample holes were lengthened and a NaI(Tl) detector was inserted for in situ measurements of the gamma-ray dose rate. Bagged samples of sediment (~60–200 g) were collected from the walls of the gamma spectrometer detector holes for water content measurements and determination of the beta dose rates (by low-level beta counting) in the laboratory.

Samples were prepared for IRSL dating using standard methods (Aitken, 1998). They were first treated with HCl acid (10%) and H_2O_2 acid (10%) to remove any traces of carbonates and organic material. Sodium polytungstate solutions of 2.70 g/cm^3 and 2.62 g/cm^3 in density were then used to remove heavy minerals and to separate quartz from feldspar, respectively. Potassium feldspar (KF) was concentrated in the feldspar separate using a solution of density 2.58 g/cm^3 and the 180–212 µm diameter grain-size fraction was isolated by dry sieving. This fraction was etched in dilute HF acid (10%) for 10 min to dissolve the alpha-irradiated rinds of the KF grains, and the etched grains were sieved again to remove grains smaller than 180 µm in diameter.

All measurements were made using a Risø TL/OSL-DA-20 equipped with a calibrated ^{90}Sr/^{90}Y beta source. The IRSL signal from 'small' KF aliquots (each aliquot containing ~30 grains) was stimulated using infrared-emitting diodes (875 nm) and the blue-violet emissions were detected using an Electron Tubes Ltd 9235QB tube fitted with Schott BG-39 and Corning 7-79 filters. Equivalent dose (D_e) values were measured using an IRSL single-aliquot regenerative dose (SAR) procedure previously tested 3 on KF grains from the Ghoghara main section and the Son River channel (Neudorf et al., 2012, submitted) (Supplementary Table 2). This procedure included measurement of the natural signal (L_n) followed by measurement of a laboratory-given test dose (T_n). A dose-response curve was then generated from the signals induced by a series of regenerative doses given in the laboratory (L_x), each followed by a test dose measurement (T_x) to correct for sensitivity changes (Galbraith et al., 1999; Wallinga et al., 2000). A zero-dose point was measured after the highest regenerative dose to assess the severity of preheat-induced thermal transfer and signal 'recuperation', and a duplicate regenerative dose was measured after the zero-dose cycle to determine the 'recycling ratio' and check that the sensitivity-correction procedure had performed adequately. For each aliquot, the L_x/T_x ratios were fitted by a single saturating exponential function to generate a sensitivity-corrected dose-response curve, onto which L_n/T_n was projected to determine the D_e. A 1.5% instrumental error was added in quadrature to the measurement uncertainty for each L_x, T_x, L_n, and T_n measurement and the D_e uncertainties were calculated by the Monte Carlo stimulation using the software package Analyst v3.24 (Duller, 2007).

IR stimulations were made for 100 s at 50°C and D_e values were determined from the IRSL counts in the first 1 s of illumination minus the mean background count rate over the last 20 s of stimulation. Aliquots were preheated at 250°C for 10 s before each IR stimulation, and given an IR bleach (for 40 s at 290°C) at the end of the natural and regenerative dose cycles. The suitability of these experimental conditions was checked and validated by preheat plateau and dose recovery tests, as reported elsewhere (Neudorf et al., 2012, submitted).

The IRSL signal measured at 50°C is well known to fade over time (Huntley and Lamothe, 2001), so tests for ‘anomalous fading’ were conducted using a SAR measurement procedure (Auclair et al., 2003) and corrections were applied to the measured ages. Each aliquot was corrected for its own fading rate so that the age distribution for each sample could be examined for evidence of incomplete bleaching before burial and/or sediment mixing afterwards, as is routinely done for quartz grains (e.g., Roberts et al., 1998; Olley et al., 2004; Jacobs et al., 2006). The fading rate of each aliquot was quantified using the *g*-value normalised to 2 days , following Huntley and Lamothe (2001), and the age of each aliquot was corrected for fading using their model (see Supplementary Table 3 for the fading measurement protocol).

2.3 Environmental dose rate determination

The IRSL age of a sample is calculated by dividing the burial dose (estimated from the D_e values) by the environmental dose rate integrated over the period of sample burial. The dose rate to KF grains consists of beta, gamma and cosmic radiation from sources external to the grains, as well as alpha and beta radiation from sources inside the grains. In this study, the internal dose rates were based on values widely used in the literature: ^{40}K and ^{87}Rb concentrations were assumed to be 12.5 ± 0.5% (Huntley and

Baril, 1997) and 400 ± 100 ppm (Huntley and Hancock, 2001), respectively, and U and Th contents were assumed to be 0.3 ± 0.1 ppm and 0.7 ± 0.1 ppm, respectively (Mejdahl, 1987). The corresponding alpha and beta dose rates were calculated using the conversion factors of Adamiec and Aitken (1998), an alpha-efficiency factor (*a*-value) of 0.09 ± 0.03 (Rees-Jones, 1995; Lang and Wagner, 1997; Banerjee et al., 2001; Lang et al., 2003) and beta-absorption factors from Brennan (2003).

External beta and gamma dose rates were measured using low-level beta counting in the laboratory and field gamma spectrometry, respectively. The external contribution from alpha particles was assumed to be negligible because of the HF acid etch given during sample preparation. The contribution of cosmic rays was estimated following Prescott and Hutton (1994), taking into consideration the latitude, longitude and altitude of the sample sites, as well as the burial depth of each sample below the modern ground surface and the density of overlying deposit. Because water attenuates beta, gamma and cosmic radiation, the water content of the sediments was measured in the laboratory and the external dose rate was calculated for an estimated long-term water content of either 5 ± 2% or 10 ± 2%, depending on the measured water content of the sample; field values ranged from 0.3 to 9.1% (Table 4). These long-term values take into consideration the free-draining nature of the sampled sediments, their collection during the dry season, and the monsoonal climate of the region. For these samples, a 1% increase in water content leads to a 1% increase in calculated age.

The external beta and gamma dose rates account for the majority (53–75%) of the environmental dose rate for these MSV samples (Table 4). The internal dose rate of 1.00 ± 0.05 Gy/ka provides a smaller contribution (21–41%) and cosmic radiation accounts for only 4–7% of the total dose rate.

3. Results

3.1 Topography and sedimentology

The topographic profiles and elevations of all IRSL sample sites are shown in Figure 4. IRSL samples were taken near the edge of each terrace at ~850 m (L-3), ~1100 m (M-2, M-4), and ~1370 m (H-1) along transect A–A' and at ~900 m (L-7), ~1220 m (M-6, M-4), ~1470 m (H-5) along transect B–B'.

Dhaba site 3 is located ~20 m above river level, and is situated in colluvium derived from the bedrock ridge on the north side of the Son River. The top of the bedrock ridge is more than 40 m above river level. On the south side of the river, the highest alluvial terrace is ~25 to ~30 m above river level and the lowest terraces are ~10 m above river level. The alluvial surface that lies at intermediate elevations (~20 m above river level) south of the dirt road forms a third terrace, on the surface of which two sandstone artefacts were found (24° 29.45'N, 82° 0.75'E) (Fig. 5). These resemble Late Acheulean/early Middle Palaeolithic artefacts that are typical of the area (Mishra et al., 1995; Haslam et al., 2011, 2012; Shipton et al., 2013). A dip in the topography appears immediately south of the road in both topographic profiles, presumably due to excavation during road construction.

The sampled sediments on the highest terrace (H-1 and H-5) are dominated by massive, yellowish brown (10 YR 5/6) silt with few calcium carbonate nodules (Fig. 5). The sediments located approximately halfway between the highest terrace and the river channel, at ~20 m above river level (M-2, M-4, M-6), are much coarser. At the site of sample M-2, they are characterized by brown (7.5 YR 4/6), matrix-supported coarse sand, pebble-gravel and cobbles. Those at the M-4 sample site are brown (7.5 YR 5/6), crudely-bedded coarse sand, granules and pebbles that are oxidized on the terrace surface, but less so below the surface. The sediments at the site of M-6 are characterised by brown (7.5 YR 5/6), unsorted, massive pebbly coarse sand, overlain by matrix-supported, coarse sandy gravel with pebbles and cobbles. The sediments in the lowest terrace (L-3 and L-7) are relatively fine-grained. Sediments at the site of sample L-3 consist of dark yellowish brown (10 YR 4/4), massive silty-fine sand with a cobble-boulder lens. The sediments at the site of sample L-7 are dominated by yellowish brown (10 YR 5/6) massive silts (Fig. 5).

The silts deposited on the highest alluvial terrace (H-1 and H-5), and the silts and silty fine sands deposited on the lowest terrace (L-3 and L-7) are likely low-energy floodplain deposits; they have sedimentological characteristics consistent with the fine member of the Baghor Formation and of the Khetaunhi Formation, respectively (Table 1). The structureless coarse sand and pebble-cobble gravels observed ~20 m above river level likely record high-energy flow and rapid deposition within a palaeo-

Son River channel dominated by bedload transport. These deposits could be considered most consistent with the sedimentological characteristics of the Patpara Formation (Table 1), but IRSL age estimates reported below suggest that they are much younger than the age of ~58–40 ka assigned by Williams et al. (2006).

3.2 IRSL chronology

The D_e values, average recycling ratios, recuperation values, fading rates, overdispersion (OD) values and fading-corrected age estimates for all samples are listed in Table 3. OD is the spread in D_e values remaining after all measurement uncertainties have been taken into account (Galbraith et al., 2005; Galbraith and Roberts, 2012). IRSL ages from two samples, GHO-2 and GHO-3, taken from alluvial sands above and below YTT ash on the north side of the Son River (Neudorf et al., 2012, submitted) are also listed for comparison. Typical IRSL decay and dose-response curves are shown in Figure 6A. The average recycling ratios are statistically consistent with unity (at 1σ), as are the ratios for each of the aliquots, suggesting that sensitivity-correction procedure performed adequately (Table 3). A typical fading plot is shown in Figure 6B and the *g*-values of all 264 aliquots from all samples (the nine listed in Table 3 and two from the Khunteli Formation type-section, Fig. 1A) is shown in Figure 6C. The average fading rate for each sample is about 3–4 % per decade and appears to be independent of sample location (Table 3, Figs. 3A, 3C).

The average recuperation values from all samples on the south side of the Son River range from ~2% to ~8% of the sensitivity-corrected natural signal, with the highest relative recuperation exhibited by the two youngest samples (L-3 and L-7), collected from the lowest terrace adjacent to the Son River (Table 3). Recuperation values from samples GHO-2 and GHO-3 are very small (<2%) because the natural signal in these relatively old samples is bright. Recuperation values of <10% are considered satisfactory, but some aliquots of samples L-3 and L-7 (eight and one, respectively) had recuperation values of >10%. For these two samples, IRSL ages were calculated after including and excluding these aliquots. The fading-corrected ages determined after rejecting these aliquots are shown in parentheses in

Table 3: the weighted mean (Central Age Model, CAM) age of sample L-3 increased slightly but not significantly (at 2σ), while the CAM and Minimum Age Model (MAM) ages for sample L-7 were unaffected (at 1σ).

Fading-corrected ages for all aliquots are displayed in Figure 7. OD values are smallest (<10%) for the samples collected from the highest terraces, and are largest for samples collected from the dirt road (~45%) and the lowest terrace (up to ~76%) (Fig. 7). OD values for quartz single-aliquot and single-grain datasets for samples known or thought to have been fully bleached at burial and not affected by post-depositional disturbance (or by significant differences in beta dose rate among grains buried at the same time) commonly have OD values of up to 20% (e.g., Galbraith et al., 2005; Jacobs et al., 2006; Arnold and Roberts, 2009). Optically stimulated luminescence (OSL) age distributions for single grains of quartz have been reported from the Ghoghara main section and the Khunteli type-section (Fig. 1A) (Neudorf et al., 2012, submitted). These have high OD values (~35–45%) and a multi-component structure, suggesting that some grains were not completely bleached before deposition and/or that older grains (derived perhaps from slumped river bank deposits) had been intermixed with younger grains transported by the river (Neudorf et al., 2012, submitted). D_e measurements of a modern sample collected from a sand bar in the Son River channel (KHUT-10) suggest that the source traps for the OSL signal in fluvially transported quartz grains are generally well bleached (Neudorf et al., submitted) and residual doses from fluvially transported KF grains are typically less than 4 Gy (Fig. 6D). Thus, the samples from the terraced alluvial deposits south of the Rehi–Son confluence with overdispersed D_e distributions (M-2, M-4, M-6, L-3 and L-7) may consist of a mixture of relatively well-bleached, river-transported grains and potentially poorly-bleached grains from slumped riverbank deposits.

The relatively low OD values of 5–7% for samples H-1 and H-5 from the highest terrace may be attributed to: 1) better bleaching conditions in a shallow water environment on a floodplain, compared to higher-energy depositional environments associated with the medium-coarse sands at lower elevations (Berger et al., 1990); and/or 2) a negligible contribution of sediment from slumped older riverbank material, due to the absence of proximal steep (palaeo-) sections of riverbank at the time of sediment deposition. Because the multi-grain aliquots of samples M-2, M-4, M-6, L-3 and L-7 may consist of partially bleached grains and/or grains derived from slumping, the MAM was used to estimate the ages of those aliquots that contain the highest proportion of grains exposed most recently to sunlight (Table 3). For comparison, ages were also calculated using the CAM, bearing in mind that such ages are equivalent to the weighted (geometric) mean and will, therefore, overestimate the burial time for samples that contain a significant proportion of partially bleached grains (Table 3). Details of the MAM and CAM are given in Galbraith et al. (1999) and Galbraith and Roberts (2012). Because the measured signal from multi-grain aliquots is the combination of signals from individual grains, the MAM estimates for samples M-2, M-4, M-6, L-3 and L-7 should conservatively be viewed as maximum IRSL ages, as they may overestimate the time since the most recently bleached grains in each of these samples were last exposed to sunlight. Neudorf et al. (submitted) measured residual doses for 24 multi-grain aliquots of KF from the modern sample (KHUT-10) using the IRSL signal. The CAM weighted mean of these residuals is 1.3 ± 0.2 Gy and the MAM estimate is 0.4 ± 0.1 Gy. These residual values have been subtracted from the CAM and MAM D_e estimates before age calculation in Table 3 to account for insufficient bleaching of grains during transport in the Son River.

4. Discussion

4.1 Revised model for alluvial deposition in the MSV

The IRSL age estimates obtained in this study suggest that the uppermost floodplain silts in the highest alluvial terrace on the south side of the Son River are ~16 ka (Table 3, Fig. 4). The partially oxidized coarse sands and gravels exposed ~5–10 m below this terrace yield maximum age estimates of ~6–8 ka, while the silts and silty sands exposed near the top of the lowermost terrace, adjacent to the Son River, yield maximum age estimates of ~1.9 ka and ~2.7 ka for samples L-3 and L-7, respectively (Table 3, Fig. 4). Pal et al. (2005) reported IRSL ages for 3 samples (BN-1, BN-2, and BN-3) from the Baghore Nala, which is the type-section for the Baghor Formation (Fig. 1A, Table 1). BN-3 was collected from the lower part of the coarse member, BN-2 from the middle part of the coarse member, and BN-1 from the upper fine member. The reported ages of 39 ± 9, 24 ± 3 and 19 ± 2 ka, respectively (Table 2) should be interpreted as minimum ages because they were not corrected for fading. Despite the latter caveat, the IRSL age of BN-1 (~19 ka) is similar to the fading-corrected IRSL ages of ~16 ka for the uppermost silts in the highest alluvial terrace sampled in this study, suggesting that these silts are correlative with the fine member of the Baghor Formation. According to the model of Williams et al. (2006), fluvial incision of the MSV alluvium commenced ~16 ka after a period of aggradation between ~39 and ~16 ka. IRSL ages for the highest terrace reported here are consistent with the termination of accumulation of Baghor fine-member silts, and the beginning of fluvial incision of the valley alluvium ~16 ka (Table 3, Fig. 4). The two maximum age estimates (~1.9 and ~2.7 ka) for the lowest terrace in the study area are slightly younger than previously reported radiocarbon age estimates from shell (3.215 ± 0.07 and 4.74 ± 0.08 ka) and charcoal (4.13 ± 0.11 ka) associated with the Khetaunhi Formation (Table 2) (Williams and Clarke, 1984).

Contrary to the predictions of the Williams et al. (2006) model (Fig. 2), our IRSL age estimates suggest that the near-surface alluvial sands and gravels ~20 m above river level are at least ~32 ka younger than the proposed age of the Patpara Formation, and at least ~8 ka younger than the proposed age of the Baghor Formation and the uppermost floodplain silts in the highest alluvial terrace (Table 3, Fig. 4). These results suggest that the intermediate (~20 m) terrace is not an erosional feature exposing sediments correlative with the Patpara Formation, but rather a depositional feature consisting of high-energy sands and gravels that were deposited during a brief aggradational phase between ~5 ka and ~16 ka. This terrace deposit contains Late Acheulean/early Middle Palaeolithic artefacts (Fig. 5H, I) that may have been eroded from underlying older sediments (i.e., the Patpara or Sihawal Formations, Table 1) before being redeposited.

In light of the new IRSL ages reported in this study, modifications to the model of Williams et al. (2006) near the Rehi–Son River confluence are introduced and illustrated in Figure 8. IRSL age estimates from the topmost terrace mark the termination of deposition of the Baghor Formation fine-member silts ~16 ka ago. Maximum IRSL age estimates of ~1.9–2.7 ka mark the termination of deposition of the

Khetaunhi Formation silts and the sands on the lowest terrace. Maximum IRSL age estimates of ~5–8 ka mark the termination of deposition of a mantle of coarse sands and gravels of unknown thickness between the highest and lowest terraces that was deposited by high-energy flow in a palaeo-Son River channel dominated by bedload transport. Because the IRSL samples dated in this study were collected from near-surface sediments, additional excavations (ideally including deep sediment cores), detailed logging of sediments, and additional numerical ages are needed to determine if there are any deposits with sedimentological characteristics and ages consistent with the Patpara, Khunteli and Sihawal Formations proposed in the stratigraphic model of Williams et al. (2006).

4.2 Son River response to past changes in SW monsoon intensity

Precipitation associated with the SW monsoon is thought to have had a prominent influence on river discharge and depositional processes in India throughout the Late Pleistocene (Goodbred, 2003), but these effects can be spatially variable (e.g., Sinha and Sarkar, 2009). River planforms, bedloads and rates of incision and deposition are inherently linked not only to climate, but also to local tectonics, channel form history, sediment supply and, in areas close to the coast, changes in relative sea level (Miller and Gupta, 1999). Our age estimates for the timing of aggradation and incision events in the MSV show some similarities to other Indian river valleys and may reflect past changes in SW monsoon intensity, as proposed previously by Williams et al. (2006). Here, we compare our age estimates for the MSV terraces to palaeoclimate records of the region.

Much of what we know of patterns of SW monsoon variability over the last 150 ka is recorded in aeolian, lacustrine and marine sedimentary records in tropical Africa, the eastern Mediterranean, and the Indian Ocean that were compiled and analyzed by Prell and Kutzbach (1987). Most of these records show four strong SW monsoon-related events that roughly coincide with the four major maxima of Northern Hemisphere summer radiation at about 10, 82, 104 and 126 ka, which fall within the present interglacial (Marine Isotope Stage, MIS, 1) and the last interglacial, MIS 5 (Fig. 9).

Palaeoclimate records from the Arabian Sea and the adjacent landmasses of Africa, Arabia and India suggest that the SW Indian monsoon was significantly weaker than at present during glacial times (~18 ka). Abrupt increases in monsoon strength appeared at ~14.5 ka and 11.4 ka and monsoon intensity reached a maximum between ~11.5 and 5.0 ka, following the recession of glaciers on, and upstream of, the Tibetan Plateau (Overpeck et al., 1996).

Clemens and Prell (2003) examined five summer-monsoon proxies (comprised of chemical, biological, and physical indicators) obtained from cores in the Arabian Sea. To extract a monsoon-related signal from the time-series data, they used principal components analysis to calculate the 'Summer Monsoon Factor', which they considered to be the most robust representation of relative amplitude in SW monsoon intensity through time (Fig. 9). The Summer Monsoon Factor is strongest during portions of non-glacial intervals MIS 3 and 5. A 35% increase in precipitation occurred between the Last Glacial Maximum (LGM) and the Holocene hypsithermal — a period driven by peak regional insolation ~9 ka and weakening glacial boundary conditions (Prell and Kutzbach, 1987). This post-LGM increase in monsoon intensity is likely responsible for an increase in the Son River discharge, and incision of the MSV floodplain, after ~16 ka (Fig. 9).

Speleothem isotope records in Oman (Fleitmann et al., 2003, 2007) generally show intensification of the SW monsoon from ~10 to 8 ka, before weakening to modern levels. Palaeoclimate records from lakes in northwest (Didwana, Nal, Lunkaransar) and northeast (Sanai) India (Wassad et al., 1984; Prasad et al, 1997; Enzel et al., 1999; Sharma et al., 2004; Prasad and Enzel, 2006) also record increased aridification at around 6–5 ka (Fig. 10). In the MSV, maximum ages ranging from 7.9 ± 1.1 to 4.8 ± 0.6 ka for the top of the middle terrace (M-2, M-4 and M-6) coincide with a relatively humid phase in all lake-level proxies (Fig. 10). This suggests that wet conditions may have been responsible for high river discharges and the transport and deposition of the coarse sand, pebble-gravel and cobbles observed in the middle terrace under a high-energy depositional environment. Subsequent northward channel migration and incision of the valley alluvium may have begun at a time when the intensity of the SW monsoon was decreasing between ~6 and ~4.7 ka (Fig. 10). The maximum ages of the top of the lowest terrace (1.9 ±

0.2 and 2.7 ± 0.2 ka) coincide with the latter part of an arid phase recorded in the Lake Sanai and speleothem isotope records (Fig. 10). Therefore, aggradation of this late Holocene terrace likely occurred during relatively arid conditions.

4.3 Comparison of the MSV and other Indian fluvial sequences

Our age estimates for the timing of aggradation and incision events in the MSV show some similarities to other Indian fluvial sequences. For example, braided channel sediments dated to ~120–100 and 70–60 ka, and widespread aeolian sediments dated to ~20–11 ka in the Mahi and Orsang basins, western India, were inferred to represent periods of weak monsoon intensity (Juyal et al., 2006). These periods of weak monsoon intensity roughly correlate with the proposed time of deposition of the Sihawal Formation (MIS 5d) and the fine member of the Baghor Formation (MIS 2), which are also associated with semi-arid conditions (Fig. 9) (Williams and Royce, 1983; Williams et al., 2006; Shipton et al., 2013). Meandering-river deposits dated to ~54–30 ka in the Sabarmati basin are thought to have aggraded during enhanced SW monsoon conditions that may be responsible for the high-energy flow regimes associated with the Patpara and Baghor coarse member gravels of the MSV (Fig. 9) (Williams and Royce, 1983; Williams et al., 2006). Incision of the Sabarmati River occurred between ~12 and 4.5 ka, an interval congruent with an increase in monsoon intensity and with early Holocene incision events in the Belan Valley, MSV and Ganga Plains (Fig. 9).

Strata recording fluvial activity over the last 100 ka in the middle Ganga Plains record major periods of fluvial aggradation that occurred about 111–59 ka (Period I), 45–30 ka (Period II), 30–23 ka (Period III), 16–11 ka (Period IV) and 2.7 ka to present (Period V) (Roy et al., 2012) (Fig. 9). Period III sediments record high-energy channel activity at ~28 ka and levee deposition about 34 and 26 ka ago, possibly associated with increased monsoon precipitation. These sediments are roughly correlative with the proposed time of deposition of the coarse member of the Baghor Formation and the time of deposition of the sediments bracketing reworked YTT ash at Ghoghara and Khunteli (Fig. 9). Period IV sediments record a phase of channel incision, followed by aggradation and channel switching in a braided depositional environment with a high sediment supply. This has been interpreted to reflect landscape instability during monsoon intensification, followed by a reduction in discharge during the Younger Dryas stade (~13–9 ka) (Roy et al., 2012). This is correlative with the time of incision of the highest (~25–30 m) terrace and subsequent aggradation of the middle (~20 m) terrace in the MSV. The late Holocene phase of aggradation in the Middle Ganges that likely occurred during a decline in monsoon intensity (Roy et al., 2012) (Fig. 9) is correlative with that associated with the lowest (10 m) terrace in the MSV (Figs. 9, 10).

Late Quaternary sequences in the southern Gangetic Plains are also thought to reflect floodplain aggradation and degradation in response to fluctuations in SW monsoon intensities, with an increase in precipitation from ~15 to 5 ka promoting incision and widespread badland formation (Gibling et al., 2005). The start of this incision event roughly correlates with that proposed for the MSV after ~16 ka (Fig. 9).

More locally, alluvial sequences in the Belan River valley, like those of the MSV, have been used as a source of palaeoclimatic information for north India (Gibling et al., 2008). The headwaters of the Belan River are in the Kaimur Hills, which lie 50 km northeast of the village of Sihawal in the MSV. The main channel drains northwest into the Tons, which in turn drains northeast into the Ganga River. Sedimentary sections along the Belan River reveal channel-based calcretes above the bedrock that are overlain by mixed-load, meandering river channel/floodplain sediments and soils (Gibling et al., 2008). Net aggradation of fluvial deposits occurred between ~85 and 16 ka (MIS 5–2) (Fig. 9): this involved mainly channel deposition from ~85 to 72 ka, followed by floodplain buildup until ~16 ka. This fining-upward stratigraphic sequence is reminiscent of the coarse and fine members of the Baghor Formation in the MSV, which are thought to record a trend toward aridification during MIS 2 (Williams et al., 2006). Some evidence for floodplain gullying and erosion at ~31–21 ka exists in the form of reworked gravel lenses in floodplain muds that may record reduced monsoonal precipitation around the LGM. Evidence for climatic instability is present in the form of fluvial and aeolian deposits at the Mahagara and Deoghat localities, which range in age from ~14 to 7 ka. Incision through terraced sediments as young as ~9 ka at

Mahagara has been interpreted to represent monsoon intensification and increased fluvial energy after 9 ka. This period of wet climatic conditions leading to incision in the Belan Valley roughly correlates with the time of aggradation of the coarse sands and gravels in the middle (~20 m) terrace in the MSV (Fig. 9). Decreasing monsoonal activity since ~6 ka is thought to be responsible for local inset terrace aggradation at Mahagara (Gibling et al., 2008), which occurred at a similar time to the aggradational event in the MSV that led to the creation of the lowest (~10 m) terrace (Fig. 9).

5. Conclusions

In this study, we set out to test the Williams et al., (2006) model of alluvial deposition for the MSV in the vicinity of the Rehi–Son confluence using cross-valley topographic profiles, field observations, and fading-corrected IRSL ages for terraced alluvial sediments. The age estimates for the highest terrace on the south side of the Son River are consistent with a previous IRSL age estimate for the fine member of the Baghor Formation (Pal et al., 2005) and with the start of incision of the MSV alluvium ~16 ka, as predicted by the Williams et al., (2006) model. Maximum age estimates from the lowest terrace are ~1.9 and 2.7 ka, which are slightly younger than the radiocarbon ages of ~3–5 ka reported by Williams and Clarke (1984) for the Khetaunhi Formation.

The IRSL age estimates for artefact-bearing coarse sands and gravels that lie at intermediate elevations (~20 m above river level) contradict what is predicted by the model of Williams et al., (2006). According to the model, these sediments should be ~58–40 ka in age and form part of the Patpara Formation, which has been exposed by fluvial erosion of the overlying Baghor Formation (Fig. 2). The maximum IRSL age estimates presented here suggest that these inset sediments were deposited no earlier than ~5–8 ka ago, during a brief aggradational phase that followed deposition of the highest alluvial surface ~16 ka ago and its subsequent incision. The Palaeolithic artefacts found in the middle terrace deposits have likely been eroded from older underlying sediments and redeposited. Incision of the MSV alluvium south of the Rehi–Son confluence began shortly after ~16 ka, probably as a result of SW monsoon intensification. The inset coarse sand and gravel deposited ~20 m above river level likely aggraded under relatively wet conditions in the early Holocene, and the lowest (~10 m) inset terrace probably aggraded under more arid conditions during the late Holocene.

The modifications to the Williams et al., (2006) model proposed here for terraced sediments south of the Rehi–Son confluence provide insights into the late Quaternary history of the Son River and the role of the SW Indian monsoon in the evolution of fluvial landforms. The numerical ages presented for the different terraces will also inform future archaeological surveys, by constraining the geomorphic context of surficial and excavated artefacts in the Middle Son Valley.

Acknowledgements

This project was funded by an ARC Discovery Project grant to R.G.R. and University of Wollongong scholarships to C.M.N. We thank S. Huot for advice and Excel macros for fading corrections, M. Petraglia and J.N. Pal for introducing us to the field sites and for archaeological advice, the local villagers of the MSV for help with field excavations and sampling, Brent Peterson, Heidi Brown and Michael Stevens for help with our surveying, GPS, DGPS and mapping enquiries, and J.-H. May for constructive comments on an earlier version of this manuscript.

References

Achyuthan, H., Quade, J., Roe, L., Placzek, C., 2007. Stable isotopic composition of pedogenic carbonates from the eastern margin of the Thar Desert, Rajasthan, India. Quaternary International 162-163, 50-60.

Adamiec, G., Aitken, M. J., 1998. Dose-rate conversion factors: update. Ancient TL 16, 37-50.

Aitken, M. J., 1998. An Introduction to Optical Dating: The dating of Quaternary sediments by the use of photon-stimulated luminescence. Oxford University Press, New York.

Arnold, L. J., Roberts, R. G., 2009. Stochastic modelling of multi-grain equivalent dose (D_e) distributions: Implications for OSL dating of sediment mixtures. Quaternary Geochronology 4, 204-230.

Auclair, M., Lamothe, M., Huot, S., 2003. Measurement of anomalous fading for feldspar IRSL using SAR. Radiation Measurements 37, 487-492.

Banerjee, D., Murray, A. S., Bøtter -Jensen, L., Lang, A., 2001. Equivalent dose estimation using a single aliquot of polymineral fine grains. Radiation Measurements 33, 73-94.

Berger, G. W., Luternauer, J. L., Clague, J. J., 1990. Zeroing tests and application of thermoluminescence dating to Fraser River delta sediments. Canadian Journal of Earth Sciences 27, 1737-1745.

Brennan, B. J., 2003. Beta doses to spherical grains. Radiation Measurements 37, 299-303.

Clark, J. D., Williams, F. M., 1987. Palaeoenvironments and prehistory in North Central India: a preliminary report. In: Jacobsen, J. (Eds.), Studies in the Archaeology of India and Pakistan. Aris and Phillips, Ltd., Warminster, pp. 19-41.

Clemens, S. C., Prell, W. L., 1991. Late Quaternary forcing of Indian Ocean summer-monsoon winds: A comparison of Fourier model and general circulation model results. Journal of Geophysical Research 96, 22683-22700.

Clemens, S. C., Prell, W. L., 2003. A 350,000 year summer-monsoon multi-proxy stack from the Owen Ridge, Northern Arabian Sea. Marine Geology 201, 35-51.

Clemens, S. C., Prell, W. L., Murray, D., Shimmield, G., Weedon, G., 1991. Forcing mechanisms of the Indian Ocean monsoon. Nature 353, 720-725.

Duller, G. A. T., 2007. Assessing the error on equivalent dose estimates derived from single aliquot regenerative dose measurements. Ancient TL 25, 15-24.

Enzel, Y., Ely, L. L., Mishra, S., Ramesh, R., Amit, R., Lazar, B., Rajaguru, S. N., Baker, V. R., Sandler, A., 1999. High-resolution Holocene environmental changes in the Thar Desert, northwestern India. Science 284, 125-128.

Fleitmann, D., Burns, S. J., Mudelsee, M., Neff, U., Kramers, J., Mangini, A., Matter, A., 2003. Holocene forcing of the Indian monsoon recorded in a stalagmite from southern Oman. Science 300, 1737-1739.

Fleitmann, D., Burns, S. J., Mangini, A., Mudelsee, M., Kramers, J., Villa, I., Neff, U., Al-Subbary, A. A., Buettner, A., Hippler, D., Matter, A., 2007. Holocene ITCZ and Indian monsoon dynamics recorded in stalagmites from Oman and Yemen (Socotra). Quaternary Science Reviews 26, 170-188.

Galbraith, R. F., Roberts, R. G., 2012. Statistical aspects of equivalent dose and error calculation and display in OSL dating: an overview and some recommendations. Quaternary Geochronology 11, 1-27.

Galbraith, R. F., Roberts, R. G., Laslett, G. M., Yoshida, H., Olley, J. M., 1999. Optical dating of single and multiple grains of quartz from Jinmium rock shelter, northern Australia: Part I, experimental design and statistical models. Archaeometry 41, 339-364.

Galbraith, R. F., Roberts, R. G., Yoshida, H., 2005. Error variation in OSL palaeodose estimates from single aliquots of quartz: a factorial experiment. Radiation Measurements 39, 289-307.

Gatti, E., Durant, A. J., Gibbard, P. L., Oppenheimer, C., 2011. Youngest Toba Tuff in the Son Valley, India: a weak and discontinuous stratigraphic marker. Quaternary Science Reviews 30, 3925-3934.

Gibling, M. R., Tandon, S. K., Sinha, R., Jain, M., 2005. Discontinuity-bounded alluvial sequences of the southern Gangetic Plains, India: aggradation and degradation in response to monsoonal strength. Journal of Sedimentary Research 75, 369-385.

Gibling, M. R., Sinha, R., Roy, N. G., Tandon, S. K., Jain, M., 2008. Quaternary fluvial and eolian deposits on the Belan River, India: paleoclimatic setting of Paleolithic to Neolithic archeological sites over the past 85,000 years. Quaternary Science Reviews 27, 391-410.

Goodbred, S. L. Jr., 2003. Response of the Ganges dispersal system to climate change: a source-to-sink view since the last interstade. Sedimentary Geology 162, 83-104.

Haslam, M., Roberts, R. G., Shipton, C., Pal, J. N., Fenwick, J. L., Ditchfield, P., Boivin, N., Dubey, A. K., Gupta, M. C., Petraglia, M., 2011. Late Acheulean hominins at the Marine Isotope Stage 6/5e transition in north-central India. Quaternary Research 75, 670-682.

Haslam, M., Harris, C., Clarkson, C., Pal, J. N., Shipton, C., Crowther, A., Koshy, J., Bora, J., Ditchfield, P., Ram, H. P., Price, K., Dubey, A. K., Petraglia, M., 2012. Dhaba: An initial report on an Acheulean, Middle Palaeolithic and microlithic locality in the Middle Son Valley, north-central India. Quaternary International 258, 191-199.

Huntley, D. J., Baril, M. R., 1997. The K content of the K-feldspars being measured in optical dating or in thermoluminescence dating. Ancient TL 15, 11-13.

Huntley, D. J., Hancock, R. G. V., 2001. The Rb contents of the K-feldspar grains being measured in optical dating. Ancient TL 19, 43-46.

Huntley, D. J., Lamothe, M., 2001. Ubiquity of anomalous fading in K-feldspars and the measurement and correction for it in optical dating. Canadian Journal of Earth Sciences 38, 1093-1106.

Jacobs, Z., Duller, G. A. T., Wintle, A. G., Henshilwood, C. S., 2006. Extending the chronology of deposits at Blombos Cave, South Africa, back to 140 ka using optical dating of single and multiple grains of quartz. Journal of Human Evolution 51, 255-273.

Jones, S. C., 2010. Palaeoenvironmental response to the ~74 ka Toba ash-fall in the Jurreru and Middle Son valleys in southern and north-central India. Quaternary Research 73, 336-350.

Jones, S. C., Pal, J. N., 2009. The Palaeolithic of the Middle Son valley, north-central India: Changes in hominin lithic technology and behaviour during the Upper Pleistocene. Journal of Anthropological Archaeology 28, 323-341.

Juyal, N., Chamyal, L. S., Bhandari, S., Bhushan, R., Singhvi, A. K., 2006. Continental record of the southwest monsoon during the last 130 ka: evidence from the southern margin of the Thar Desert, India. Quaternary Science Reviews 25, 2632-2650.

Lang, A., Wagner, G. A., 1997. Infrared stimulated luminescence dating of Holocene colluvial sediments using the 410 nm emission. Quaternary Science Reviews 16, 393-396.

Lang, A., Hatté, C., Rousseau, D.-D., Antoine, P., Fontugne, M., Zöller, L., Hambach, U., 2003. High-resolution chronologies for loess: comparing AMS ^{14}C and optical dating results. Quaternary Science Reviews 22, 953-959.

Mandal, D., 1983. A note on the radiocarbon dates from the Middle Son Valley. In: Sharma, G. R., Clark, J.D. (Eds.), Palaeoenvironments and Prehistory in the Middle Son Valley. A. H. Wheeler & Co, Private Limited, Allahabad, pp. 185-289.

Mejdahl, V., 1987. Internal radioactivity in quartz and feldspar grains. Ancient TL 5, 10-17.

Miller and Gupta, 1999. Varieties of fluvial form. J. Wiley, New York.

Mishra, S., Venkatesan, T. R., Rajaguru, S. N., Somayajulu, B. L. K., 1995. Earliest Acheulian industry from Peninsular India. Current Anthropology 36, 847-851.

Neudorf, C. M., Roberts, R. G, Jacobs, Z., 2012. Sources of overdispersion in a K-rich feldspar sample from north-central India: insights from D_e, K content and IRSL age distributions for individual grains. Radiation Measurements 47, 696-702.

Neudorf, C. M., Roberts, R. G., Jacobs, Z. Assessing the time of final deposition of Youngest Toba Tuff deposits in the Middle Son Valley, northern India, from optical dating of quartz and feldspar grains. Palaeogeography, Palaeoclimatology, Palaeoecology (submitted).

Olley, J. M., Pietsch, T., Roberts, R. G., 2004. Optical dating of Holocene sediments from a variety of geomorphic settings using single grains of quartz. Geomorphology 60, 337-358.

Overpeck, J., Anderson, D., Trumbore, S., Prell, W. L., 1996. The southwest Indian Monsoon over the last 18,000 years. Climate Dynamics 12, 213-225.

Pal, J. N., Williams, M. A. J., Jaiswal, M., Singhvi, A. K., 2005. Infra red stimulated luminescence ages for prehistoric cultures in the Son and Belan Valleys, North Central India. Journal of Interdisciplinary Studies in History and Archaeology 1, 51-62.

Prasad, S., Enzel, Y., 2006. Holocene paleoclimates of India. Quaternary Research 66, 442-453.

Prell, W. L., Kutzbach, J. E., 1987. Monsoon variability over the past 150,000 years. Journal of Geophysical Research 92, 8411-8425.

Prescott, J. R., Hutton, J. T., 1994. Cosmic ray contributions to dose rates for luminescence and ESR dating: large depths and long-term time variations. Radiation Measurements 23, 497-500.

Rees-Jones, J., 1995. Optical dating of young sediments using fine-grain quartz. Ancient TL 13, 9-14.

Roberts, R., Bird, M., Olley, J., Galbraith, R., Lawson, E., Laslett, G., Yoshida, H., Jones, R., Fullagar, R., Jacobsen, G., Hua, Q., 1998. Optical and radiocarbon dating at Jinmium rock shelter in northern Australia. Nature 393, 358-362.

Roy, N. G., Sinha, R., Gibling, M. R., 2012. Aggradation, incision and interfluve flooding in the Ganga Valley over the past 100,000 years: Testing the influence of monsoonal precipitation. Palaeogeography, Palaeoclimatology, Palaeoecology 356-357, 38-53.

Sharma, G. R., Clark, J. D., 1982. Palaeo-environments and prehistory in the Middle Son Valley, northern Madhya Pradesh. Man and the Environment 6, 56-62.

Sharma, G. R., Clark, J. D. 1983. Palaeoenvironments and Prehistory in the Middle Son Valley, Madhya Pradesh, North-Central India. A. H. Wheeler and Co. Private Limited, Allahabad.

Sharma, S., Joachimski, M., Sharma, M., Tobschall, H. J., Singh, I. B., Sharma, C., Chauhan, M. S., Morgenroth, G., 2004. Lateglacial and Holocene environmental changes in Ganga plain, Northern India. Quaternary Science Reviews 23, 145-159.

Shipton, C., Clarkson, C., Pal, J. N., Jones, S. C., Roberts, R. G., Harris, C., Gupta, M. C., Ditchfield, P. W., Petraglia, M. D., 2013. Generativity, hierarchical action and recursion in the technology of the Acheulean to Middle Palaeolithic transition: a perspective from Patpara, the Son Valley, India. Journal of Human Evolution 65, 93-108.

Singhvi, A. K., Williams, M. A. J., Rajaguru, S. N., Misra, V. N., Chawla, S., Stokes, S., Chauhan, N., Francis, T., Ganjoo, R. K., Humphreys, G. S., 2010. A ~200 ka record of climatic change and dune activity in the Thar Desert, India. Quaternary Science Reviews 29, 3095-3105.

Sinha, R., Sarkar, S., 2009. Climate-induced variability in the Late Pleistocene–Holocene fluvial and fluvio-deltaic successions in the Ganga plains, India: A synthesis. Geomorphology 113, 173-188.

Sirocko, F., Sarnthein, M., Erlenkeuser, H., Lang, H., Arnold, M., Duplessy, J. C., 1993. Century-scale events in monsoonal climate over the past 24000 years. Nature 364, 322-324.

Smith, V. C., Pearce, N. J. G., Matthews, N. E., Westgate, J. A., Petraglia, M. D., Haslam, M., Lane, C. S., Korisettar, R., Pal, J. N., 2011. Geochemical fingerprinting of the widespread Toba tephra using biotite compositions. Quaternary International 246, 97-104.

Srivastava, P., Juyal, N., Singhvi, A. K., Wasson, R. J., Bateman, M. D., 2001. Luminescence chronology of river adjustment and incision of Quaternary sediments in the alluvial plain of the Sabarmati River, north Gujarat, India. Geomorphology 36, 217-229.

Storey, M., Roberts, R. G., Saidin, M., 2012. Astronomically calibrated $^{40}Ar/^{39}Ar$ age for the Toba supereruption and global synchronization of late Quaternary records. Proceedings of the National Academy of Sciences of the USA 109, 18684-18688.

Waelbroeck, C., Labeyrie, L., Michel, E., Duplessy, J.C., McManus, J.F., Lambeck, K., Balbon, E., Labracherie, M., 2002. Sea-level and deep water temperature changes derived from benthic foraminifera isotopic records. Quaternary Science Reviews 21, 295-305.

Wallinga, J., Murray, A., Wintle, A., 2000. The single-aliquot regenerative-dose (SAR) protocol applied to coarse-grain feldspar. Radiation Measurements 32, 529-533.

Williams, M. A. J., 2012. Did the 73 ka Toba super-eruption have an enduring effect? Insights from genetics, prehistoric archaeology, pollen analysis, stable isotope geochemistry, geomorphology, ice cores, and climate models. Quaternary International 269, 87-93.

Williams, M. A. J., Clarke, M. F., 1984. Late Quaternary environments in north-central India. Nature 308, 633-635.

Williams, M. A. J., Clarke, M. F., 1995. Quaternary geology and prehistoric environments in the Son and Belan Valleys, north central India. Geological Society of India Memoir 32, 282-308.

Williams, M. A. J., Royce, K., 1982. Quaternary geology of the Middle Son Valley, North Central India: Implications for prehistoric archaeology. Palaeogeography, Palaeoclimatology, Palaeoecology 38, 139-162.

Williams, M. A. J., Royce, K., 1983. Alluvial History of the Middle Son Valley, North Central India. In: Sharma, G. R., Clark, J. D. (Eds.), Palaeoenvironments and Prehistory in the Middle Son Valley, Madhya Pradesh, North-Central India. A. H. Wheeler & Co, Allahabad, pp. 9-21.

Williams, M. A. J., Pal, J. N., Jaiswal, M., Singhvi, A. K., 2006. River response to Quaternary climatic fluctuations: evidence from the Son and Belan valleys, north-central India. Quaternary Science Reviews 25, 2619-2631.

Williams, M. A. J., Ambrose, S. H., van der Kaars, S., Ruehlemann, C., Chattopadhyaya, U., Pal, J., Chauhan, P. R., 2009. Environmental impact of the 73 ka Toba super-eruption in South Asia. Palaeogeography, Palaeoclimatology, Palaeoecology 284, 295-314.

Zimmerman, D. W. 1971: Thermoluminescent dating using fine grains from pottery. Archaeometry 13, 29-52.

List of Figures

Figure 1. A. The Middle Son Valley (MSV) and the locations of archaeological sites and preserved Youngest Toba Tuff (YTT) ash along the banks of the Son River (after Sharma and Clark, 1983). B. View south across the Son River from Dhaba sites 2 and 3 of Haslam et al. (2012).

Figure 2. Schematic cross-section of the MSV looking east from the Rehi–Son confluence, modified after Williams and Royce (1983) to include the new Khunteli Formation introduced by Williams et al. (2006). Formation ages are after Williams et al. (2006). The ages of the Patpara and Khunteli formations include a question mark as these are debated (see text for details). A "depositional surface" is defined here as one in which the most recently deposited stratigraphic formation is still preserved after lateral migration of the channel and/or incision of the river into the floodplain. An "erosional surface" is one in which one or more stratigraphic formations have been eroded, exposing one or more of the older, underlying stratigraphic formations. It is possible that some erosion has occurred on all alluvial surfaces immediately before lateral migration of the channel and/or incision of the river into the floodplain.

Figure 3. A. The MSV and the locations of archaeological sites along the banks of the Son River (after Sharma and Clark, 1983). (B) and (C) show WorldView-1 50 cm panchromatic imagery of the study area. The white dashed lines in (C) delineate the prominent WSW–ENE trending terrace escarpment ~500–700 m south of the Son River and the gentle break in topography parallel to the dirt road north of this. Yellow lines delineate topographic survey transects A–A' and B–B'. IRSL sample sites are indicated by yellow dots, and the three archaeological sites of the Dhaba locality of Haslam et al. (2012) are indicated by black dots.

Figure 4. Topographic profiles A–A' and B–B' showing the current river floodplain and the IRSL age estimates of the near-surface alluvial sediments. The elevation of YTT at the Ghoghara main section

is shown in B–B'; the sediments below and above the reworked YTT at this section are estimated to have been deposited ~36–44 ka ago (Neudorf et al., submitted). See Figure 3C for a plan view of the traverses and IRSL sample locations.

Figure 5. Alluvial sediments sampled for luminescence dating. Samples H-1 (A) and H-5 (B) were taken from the highest terrace south of the Son River. Samples M-2 (C), M-4 (D) and M-6 (E) were taken beside the dirt road, ~240–340 m away from the river channel. Samples L-3 (F) and L-7 (G) were taken in gullies near the edge of the lowest terrace. Both sides (H, I) of two Late Acheulean/early Middle Palaeolithic stone artefacts found on the ground surface near sample site M-4. Metre stick with 20 cm subdivisions for scale. Refer to Figure 3C and Supplementary Table 1 for IRSL sample locations.

Figure 6. A. Typical IRSL decay curve and dose-response curve (inset graph) for a single aliquot of KF grains from sample H-1. For each aliquot, the IRSL signal in the initial 1 s of stimulation minus the mean background count from the last 20 s of stimulation (intervals denoted by grey bands in (A)) was used to calculate the D_e value and estimate the fading rate. B. A typical fading plot (data for a single aliquot of sample H-1). C. Calculated g-values for individual aliquots of all samples in Table 3, as well as two samples (KHUT-1 and KHUT-4) collected from above and below YTT ash at the Khunteli Formation type-section (Fig. 1A) (n = 264). D. D_e distribution for single aliquots of KF grains from a modern sand bar in the middle of the Son River (sample KHUT-10). The grey shaded area should capture 95% of the points if they were statistically consistent (at 2σ) with a D_e of 0 Gy (Galbraith and Roberts, 2012).

Figure 7. Fading-corrected IRSL ages for individual aliquots of each sample, displayed as radial plots. The grey shaded area is centered on the CAM age estimate and should capture 95% of the points if they were statistically consistent with the CAM age at 2σ (Galbraith and Roberts, 2012). The black line is centered on the MAM age estimate.

Figure 8. Schematic cross-section of the MSV looking east from the Rehi–Son confluence (modified after Williams and Royce, 1983). Proposed ages of near-surface sediments on the south side of the Son River are based on the IRSL age estimates obtained in this study (Table 3). Sediments consistent with the age and sedimentology of the Sihawal and/or Patpara Formations of Williams et al. (2006) may

exist at some depth below the surface (see text for explanation). See Figure 2 caption for the definition of "depositional surface".

Figure 9. The Summer Monsoon Factor of Clemens and Prell (2003) based on stacked Arabian Sea core records and the modelled SW Indian monsoon record from Prell and Kutzbach (1987). The boundaries between marine isotope stages (MIS) are from Waelbroeck et al. (2002). Periods of alluvial aggradation and incision for the Middle Ganga Plains (Roy et al., 2012), the southern Ganga Plains (Gibling et al., 2005), the Sabarmati River (Srivastava et al., 2001), the Belan Valley (Gibling et al., 2008) and the Middle Son Valley (Williams et al., 2006) are indicated by black bars. Arrows mark incision events. The timing of alluviation and incision is approximate. The Middle Son Valley stratigraphic formation age estimates are from Williams et al. (2006) and the IRSL age estimates are from Neudorf et al. (submitted) and this study (Table 3).

Figure 10. NW Indian lacustrine records from Wassad et al. (1984) (A), Prasad et al. (1997) (B), and Enzel et al. (1999) (C) as interpreted by Prasad and Enzel (2006), and the lacustrine record from NE India from Sharma et al. (2004) (D) as interpreted in this study. E. The speleothem isotope record from Oman (Fleitmann et al., 2003). The interpretation of the NW India lacustrine records is presented only in relative wetness terms for the different basins; the absolute water levels of lake or ground water or their transfer to values of precipitation are still problematic (Prasad and Enzel, 2006). The Oman cave record was proposed to represent variations in SW monsoon rainfall. The arrow indicates the time when the trend towards aridity began, as inferred by Prasad and Enzel (2006). The grey shaded areas represent the IRSL age estimates of the tops of the lowest (~10 m) and middle (~20 m) terraces across from the Rehi–Son confluence in the Middle Son Valley (this study).

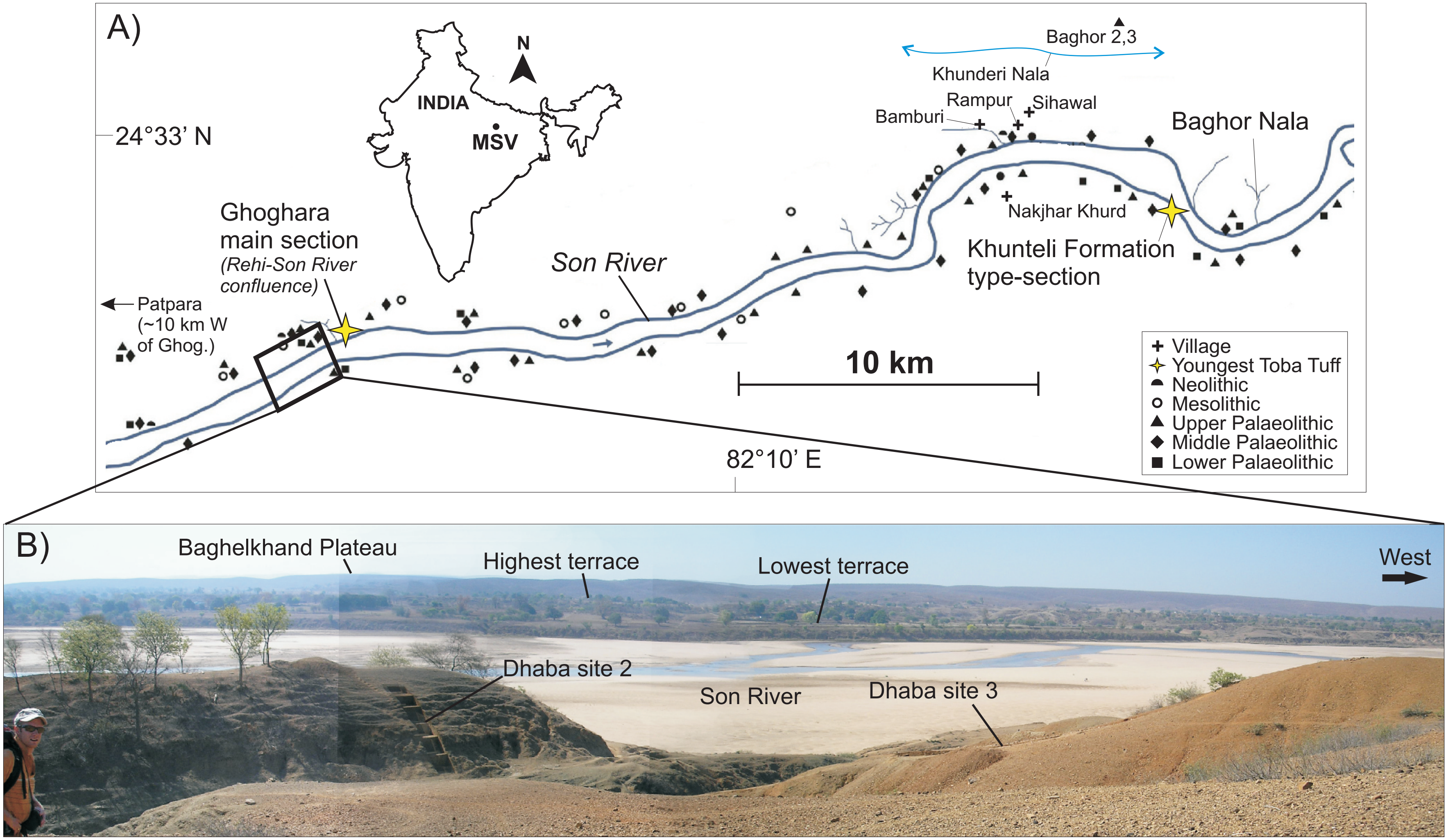

Figure 1. A) The Middle Son Valley (MSV) and the locations of archaeological sites and preserved YTT ash along the banks of the Son River after Sharma and Clark (1983). B) View south across the Son River from Dhaba sites 2 and 3 of Haslam *et al.* (2012).

SEE END OF MANUSCRIPT FOR UPDATED FIGURE CAPTIONS.

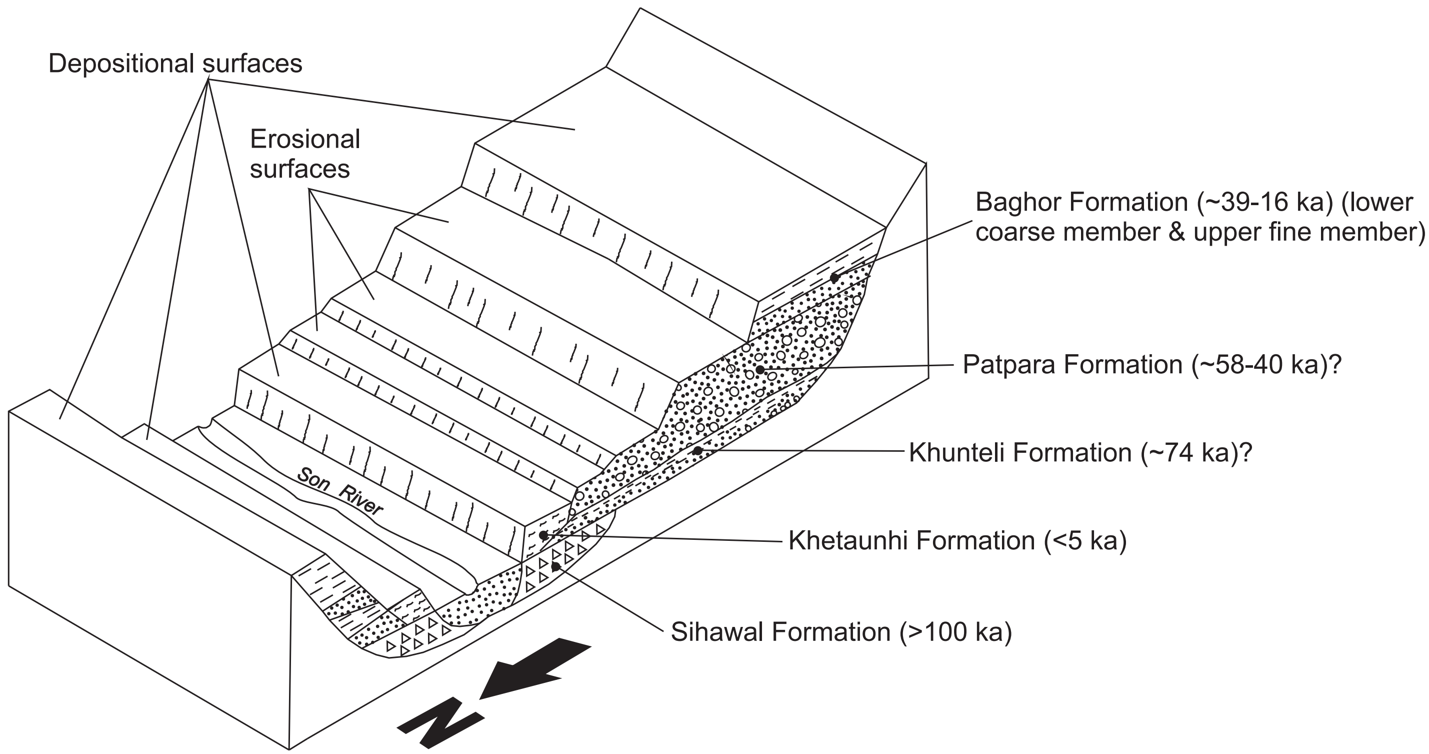

Figure 2. Schematic cross-section of the Middle Son Valley looking east from the Rehi-Son confluence, modified after Williams and Royce (1983) to include the new Khunteli Formation introduced by Williams *et al.* (2006). Formation ages are after Williams *et al.* (2006). The ages of the Patpara and Khunteli formations include a question mark as these are debated (see text for details). A "depositional surface" is defined here as one in which the most recent stratigraphic formation deposited is still preserved after lateral migration of the channel and/or incision of the river into the floodplain, while an "erosional surface" is one in which one or more stratigraphic formations have been eroded, exposing one or more older underlying stratigraphic formations. It is possible that some erosion has occurred on all alluvial surfaces immediately before lateral migration of the channel and/or incision of the river into the floodplain.

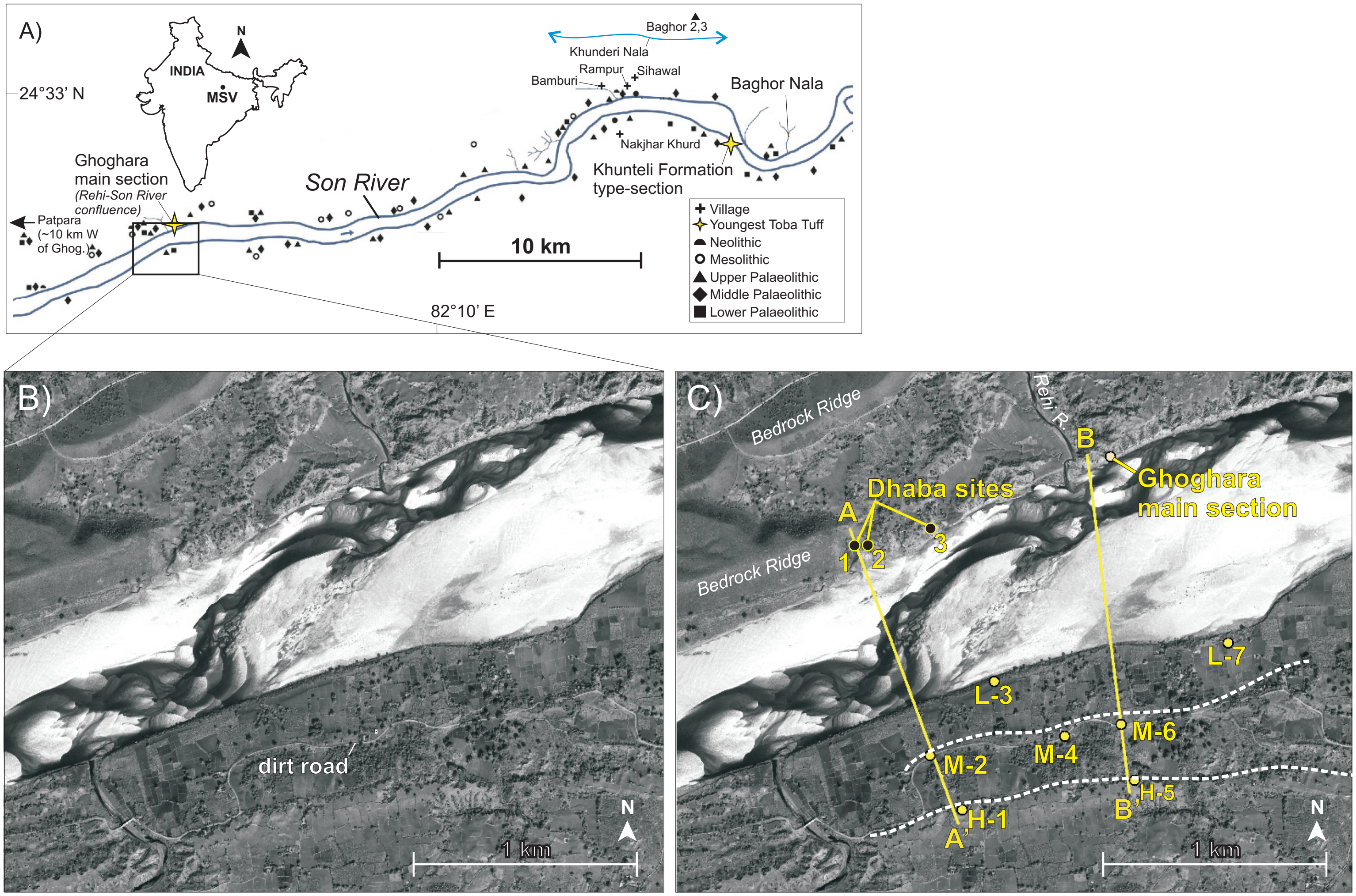

Figure 3. a) The Middle Son Valley (MSV) and the locations of archaeological sites along the banks of the Son River after Sharma and Clark (1983). b) WorldView-1 50 cm panchromatic imagery of the study area. c) White dashed lines delineate the prominent WSW-ENE trending terrace escarpment ~500-700 m south of the Son River and the gentle break in topography parallel to the dirt road north of this. Yellow lines delineate topographic survey transects A-A' and B-B'. Luminescence sample sites are indicated by yellow dots, and the three archaeological sites of the Dhaba locality of Haslam *et al.* (2012) are indicated by black dots.

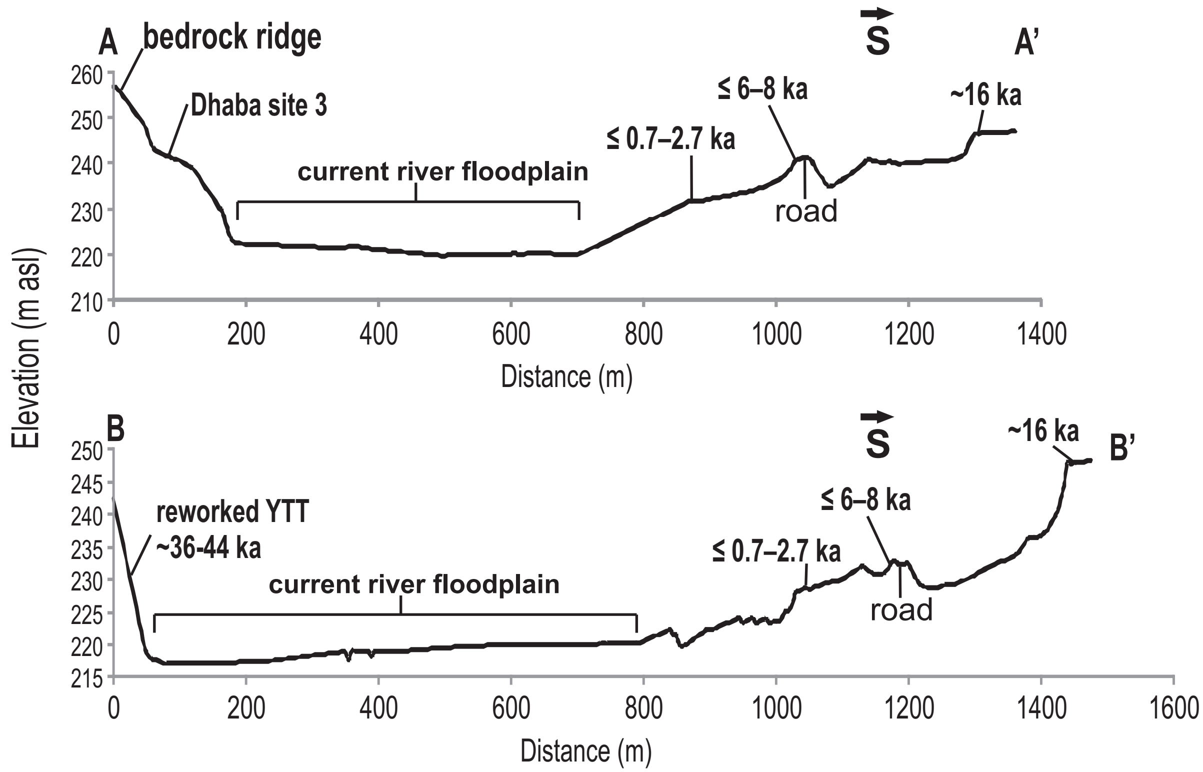

Figure 4. Topographic profiles A-A' and B-B'. The current river floodplain, as well as IRSL age estimates of near-surface alluvial sediments are indicated. The elevation of YTT as in the Ghoghara main section is shown in B-B'. The depositional age of the YTT has been estimated to be ~36-44 ka (Neudorf et al. in prep). See Figure 3c for a plan view of the traverses and IRSL sample locations.

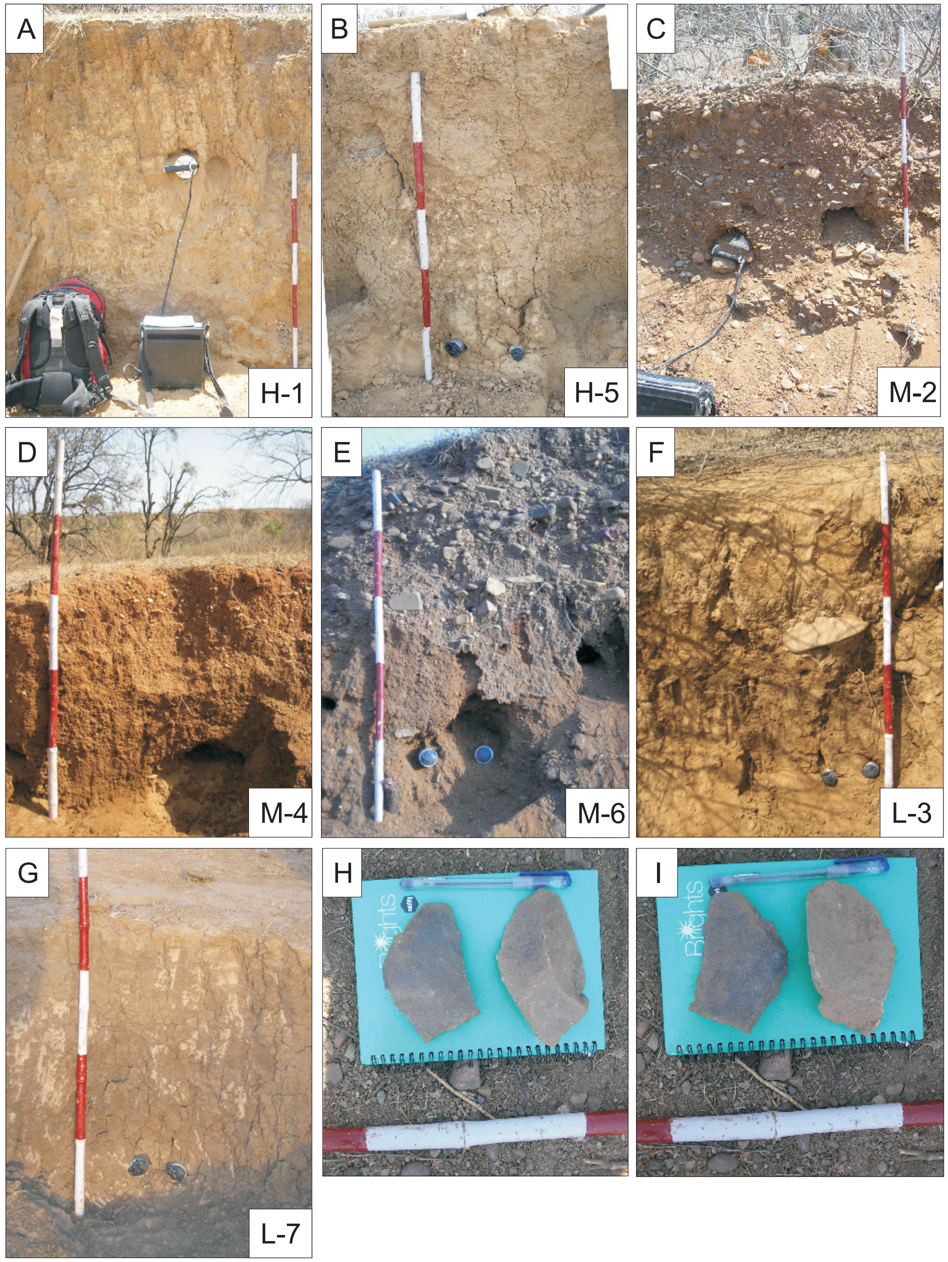

Figure 5. Alluvial sediments sampled for luminescence dating. Samples H-1 (A) and H-5 (B) were taken from the highest terrace south of the Son River. Samples M-2 (C), M-4 (D) and M-6 (E) were taken beside the dirt road ~240-340 m away from the river channel. Samples L-3 (F) and L-7 (G) were taken in gullies near the edge of the lowest terrace. The front (H) and reverse (I) sides of two Late Acheulean/early Middle Palaeolithic artefacts made of sandstone found on the ground surface near sample site M-4. Metre stick with 20 cm subdivisions for scale. Refer to Figure 3c for IRSL sample locations.

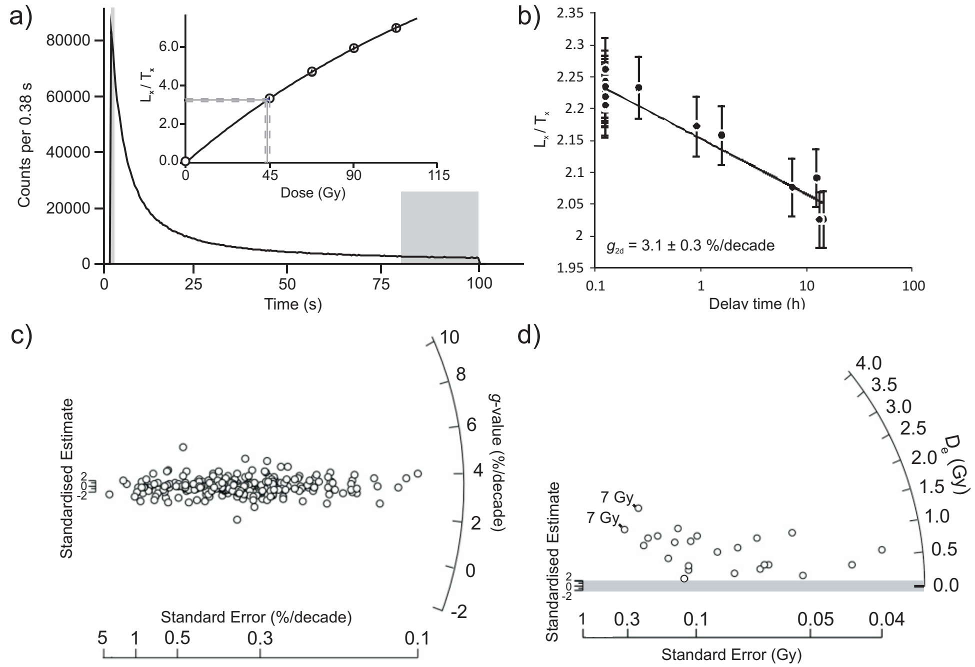

Figure 6. a) Typical IRSL decay curve and dose-response curve (inset graph) for sample H-1. The IRSL signal in the first 1 s of stimulation minus the mean background from the last 20 s of stimulation (grey shading in 'a') was used to calculate the D_e values and estimate the fading rates. b) A typical fading plot for one aliquot (from sample H-1). c) Calculated *g*-values for aliquots from all samples in Table 4, as well as two samples (KHUT-1 and KHUT-4) collected from above and below YTT ash at the Khunteli Formation type-section (Fig. 1a) (n=264). d) A KF aliquot De distribution from a sample collected from a modern sand bar in the middle of the Son River (KHUT-10). The grey shaded area should capture 95% of the points if they were statistically consistent with 0 Gy (Galbraith et al. 1999).

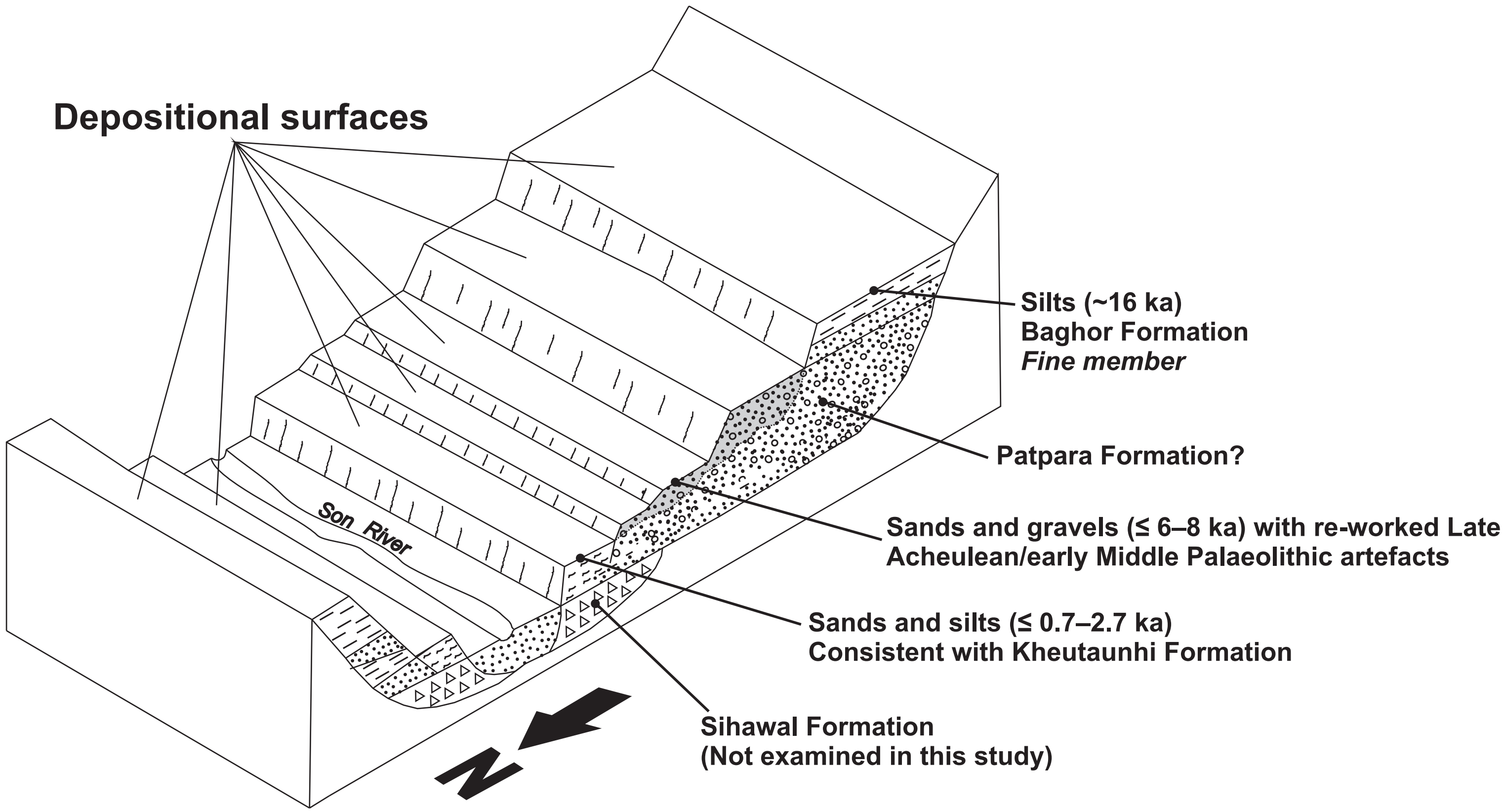

Figure 8. Schematic cross-section of the Middle Son Valley looking east from the Rehi-Son confluence, modified after Williams and Royce (1983). Proposed ages of near-surface sediments on the south side of the Son River are based on IRSL age estimates from this study. Sediments consistent in age and sedimentology of the Patpara Formation of Williams *et al.* (2006) may exist at some depth below the surface (see text for explanation). See Figure 2 for a specific definition of "depositional surface".

a) Sample H-1 (highest terrace)
OD = 7 ± 2%

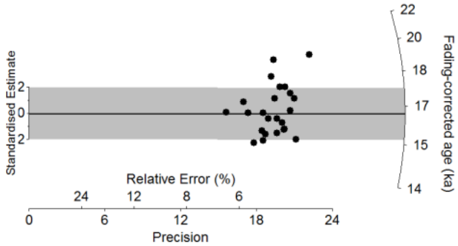

b) Sample M-2 (dirt road)
OD = 47 ± 7%

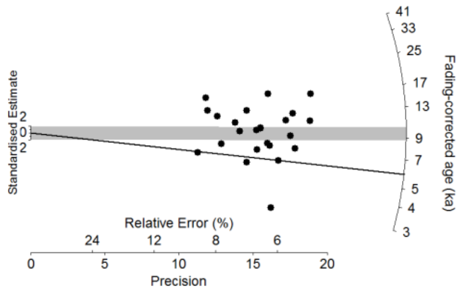

c) Sample L-3 (lowest terrace)
OD = 79 ± 11%

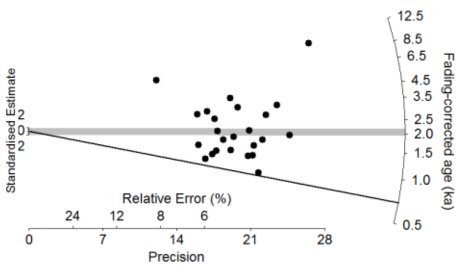

d) Sample M-4 (dirt road)
OD = 48 ± 7%

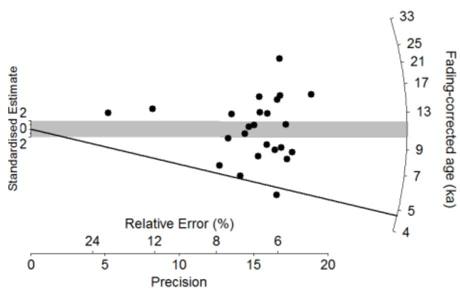

e) Sample H-5 (highest terrace)
OD = 5 ± 2%

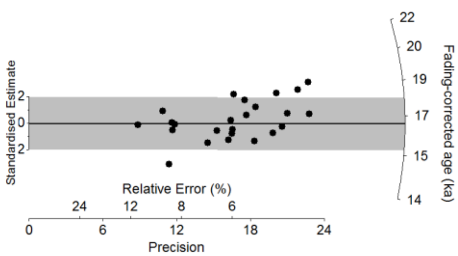

f) Sample M-6 (dirt road)
OD = 42 ± 7%

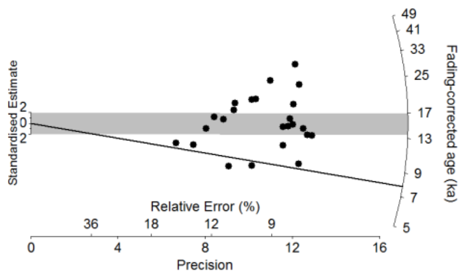

g) Sample L-7 (lowest terrace)
OD = 44 ± 6%

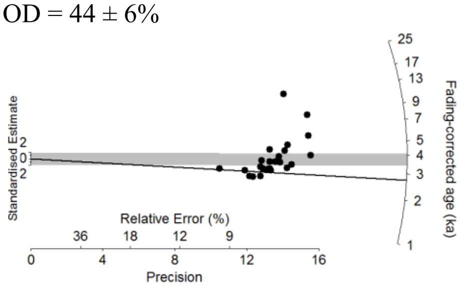

Figure 7. $IRSL_{50}$ fading-corrected aliquot ages for each sample, displayed on a radial plot. The grey shaded area is centered on the CAM age estimate and should capture 95% of the points if they were statistically consistent with each other (Galbraith et al. 1999). The black line is centered on the MAM age estimate.

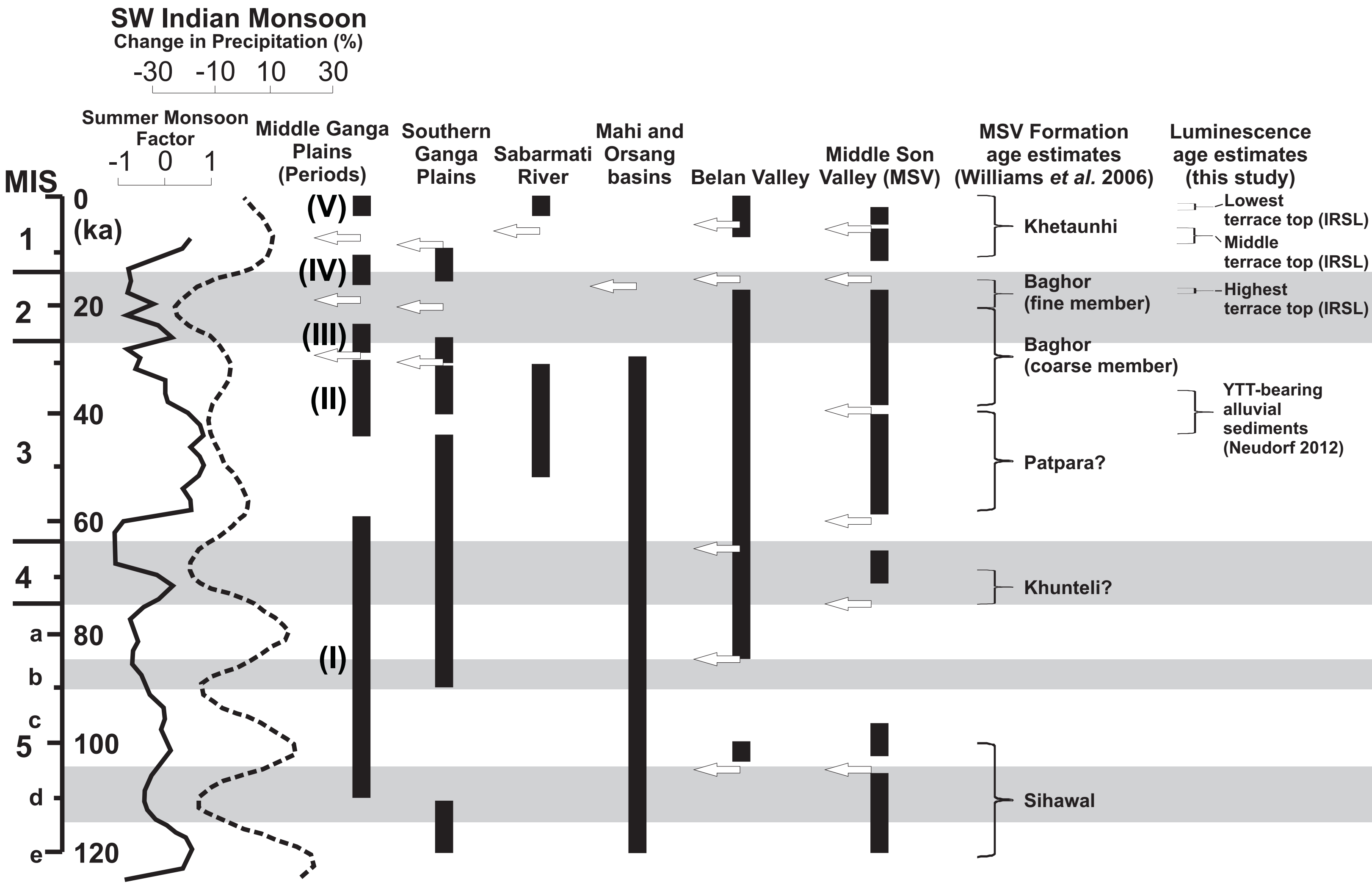

Figure 9. The Summer Monsoon Factor of Clemens and Prell (2003) based on stacked Arabian Sea core records and the modelled SW Indian monsoon record from Prell and Kutzbach (1987). The boundaries between marine isotope stages (MIS) are from Waelbroeck *et al.* (2002). Periods of alluvial aggradation and incision for the Middle Ganga Plains (Roy *et al.* 2011), the southern Ganga Plains (Gibling *et al.* 2005), the Sabarmati River (Srivastava *et al.* 2001) the Belan Valley (Gibling *et al.* 2008) and the Middle Son Valley (Williams *et al.* 2006) are indicated by black bars. Arrows mark incision events. The timing of alluviation and incision is approximate. The Middle Son Valley stratigraphic formation age estimates are from Williams *et al.* (2006) and the luminescence age estimates are from Neudorf 2012 and this study (Table 3).

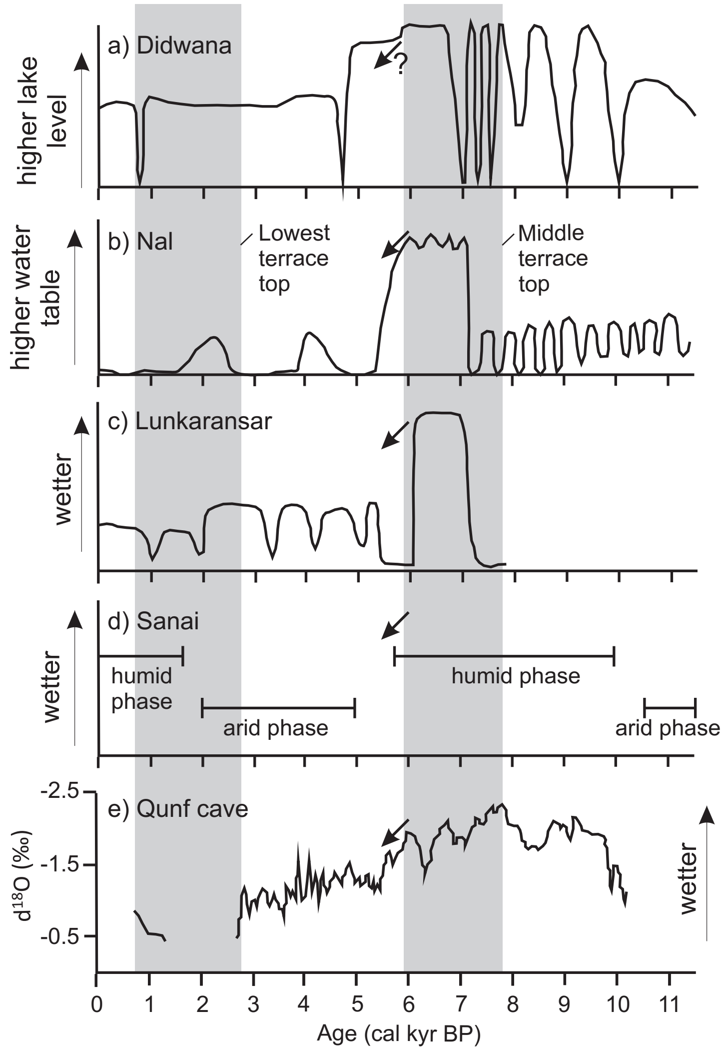

Figure 10. NW Indian lacustrine records from Wasson *et al.* (1984) (a), Prasad *et al.* (1997) (b), and Enzel *et al.* (1999) (c) as interpreted by Prasad and Enzel (2006), and the lacustrine record from NE India from Sharma *et al.* (2004) (d) as interpreted in this study. e) The speleothem isotope record from Oman (Fleitmann *et al.* 2003). The interpretation of the NW India lacustrine records is presented only in relative wetness terms for the different basins; the absolute water levels of lake or ground water or their transfer to values of precipitation are still problematic (Prasad and Enzel 2006). The Oman cave record was proposed to represent variations in SW monsoon rainfall. The arrow indicates the time when the trend towards aridity began as inferred by Prasad and Enzel (2006). The grey shaded areas represent the luminescence age estimates of the tops of the lowest (~10 m) and middle (~20 m) terraces across from the Rehi-Son confluence in the Middle Son Valley (this study).

Table 1. Stratigraphic formations in the Middle Son Valley and their artefact and fossil assemblages and estimated ages (after Williams and Royce, 1982; Pal et al., 2005; and Williams et al., 2006).

Formation	Artefact/fossil assemblage	Sedimentological characteristics	Estimated age
Sihawal	Lower Palaeolithic (Acheulean) artefacts	Rests unconformably on eroded Proterozoic bedrock and consists of angular mudstone, sandstone and quartzite clasts (up to 50 cm in diameter) set in a matrix of structurelss, mottled grey and brown silty clay. Locally, the boulder clay is overlain by mottled grey and brown silty clay loam with an erosional upper contact with the Patpara Formation. Maximum observed thickness of 1.5 m.	≥100 ka
Khunteli[1]		Consists of pale yellow brown unconsolidated medium sand with a discontinuous bed of volcanic ash ~1.5 m thick. This ash-rich sand is unconformably overlain by gravel, which, in turn, is conformably overlain by a series of calcareous clays, loams and sands.	~74 ka?
Patpara[2]	Fresh and abraded Middle Palaeolithic artefacts	Unconformably overlies the Sihawal Formation. Dark reddish medium to very coarse sands, granules, pebbles and gravels consisting of locally derived sandstone, mudstone and quartzite, as well as agate, chalcedony, and other microcrystalline silicic rocks derived from the Deccan Trap Basalts in the headwater region of the Son River. Structureless or crudely developed undulose lamination, and partially cemented by iron oxide. Overlain by dark reddish-brown indurated silty clay in places, but this is commonly eroded by the overlying Baghor Formation. Maximum exposed thickness of 10 m.	~58 to ~40 ka?
Baghor *coarse lower member*	Rolled and abraded Middle Palaeolithic artefacts and well preserved fossils, including buffalo, hippo, crocodile, antelope, elephant and tortoise	Unconsolidated cross-bedded sand with granules, pebbles and cobbles composed mainly of quartz and minor concentrations of sandstone, mudstone, quartzite, chalcedony, and chert. Calcium carbonate cementation is concentrated along planar bedding surfaces and foreset laminae. Maximum thickness ~10 m.	~39 to ~20 ka
Baghor *finer upper member*	Fresh Upper Palaeolithic artefacts	Forms the highest aggradational surface in the Son Valley, and rests conformably on the underlying coarse member of the Baghor Formation. Horizontal layers of silts, clays, and less commonly, fine sands, which vary in thickness from 1 to 4 m and continue laterally for 23 km. Blocky or massive structure and irregular pedogenic calcium carbonate nodules, tubules and plates at well- defined levels. These become more heavily concentrated near the top.	~20 to ~16 ka
Khetaunhi	Microlithic and Neolithic artefacts	Forms a prominent aggradational terrace ~10 m above river level. Interbedded silts and clays with occasional fine sand beds. Maximum thickness ~10 m.	<10 ka

[1]The introduction of the Khunteli Formation has recently been deemed problematic on the grounds that few exposures have been identified with confidence, and its stratigraphic position relative to other formations has not been demonstrated clearly (Jones and Pal, 2009; Williams, 2012).

[2]The proposed age of the Patpara Formation was originally based on one IRSL age of 58 ± 6 ka. The validity of this age has been recently questioned in light of archaeological evidence, the stratigraphic context of the IRSL sample, and the fact that the IRSL age was not corrected for fading (Jones and Pal, 2009).

Table 2. Numerical ages for Middle Son Valley deposits, updated from Jones and Pal (2009). See Figure 1A for site locations.

Date (ka) (^{14}C ka calBP[1])	Lab no.	Method/location	Stratigraphic formation (associated archaeology)	Reference
3.215 ± 0.07 (3.26–3.63)	Beta 4879	^{14}C (shell)/ not specified	Khetaunhi (Neolithic)	Williams and Clarke (1984)
4.13 ± 0.11 (4.25–5.00)	Beta 6414	^{14}C (charcoal)/ not specifid	Khetaunhi (Neolithic)	Williams and Clarke (1984)
4.74 ± 0.08 (5.31–5.61)	Beta 6415	^{14}C (shell)/ not specified	Khetaunhi (Neolithic)	Williams and Clarke (1984)
5.305 ± 0.09 (5.91–6.28)	SUA 1422	^{14}C ($CaCO_3$)/ not specified	Baghor fine member	Mandal (1983) Williams and Royce (1982)
6.66 ± 0.18	PRL 714	^{14}C (charcoal) Baghor 3	Baghor fine member (microliths)	Mandal (1983)
8.33 ± 0.22	PRL 715	^{14}C (charcoal)\ Baghor 2	Baghor fine member (microliths)	Mandal (1983)
11.87 ± 0.12 (13.4–14.0)	Beta 4793	^{14}C (shell)/ Rampur	Baghor fine member or coarse member (Upper Palaeolithic)	Williams and Clarke (1984) Clark and Williams (1987)
12.81 +0.22/-0.21	PRL 711	^{14}C (pedogenic $CaCO_3$)/ Baghor Nala	Baghor coarse member	Mandal (1983)
13.145 ± 0.14 (15.1–16.1)	SUA 1420	^{14}C (pedogenic $CaCO_3$)/ Baghor Nala	Baghor coarse member	Mandal (1983) Williams and Royce (1982)
19 ± 2	BN-1	IRSL (coarse-grained feldspar)/ Baghor Nala	Baghor fine member	Pal *et al.* (2005) Williams *et al.* (2006)
20.135 ± 0.22 (23.45–24.75)	Beta 4791	^{14}C (shell)/ Khunderi Nala	Baghor fine member?	Williams and Clarke (1984, 1995)
24 ± 3 (or 22 ka in Pal et al. (2005))	BN-2	IRSL (coarse-grained feldspar)/ Baghor Nala	Baghor coarse member	Pal *et al.* (2005) Williams *et al.* (2006)
26.1 ± 5.4	Alpha 898	TL (polymineral fine grains)/ Nakhjar Khurd	Baghor coarse member	Pal *et al.* (2005)
26.25 ± 0.42 (29-~31)	Beta 4793	^{14}C (shell)/ Rampur	Baghor coarse member? (Upper Palaeolithic?)	Williams and Clarke (1984, 1995) Clark and Williams (1987)
39 ± 9	BN-3	IRSL (coarse-grained feldspar)/ Baghor Nala	Baghor coarse member	Pal *et al.* (2005) Williams *et al.* (2006)
26.85 +0.82/-0.75	PRL 710	^{14}C (pedogenic $CaCO^3$)/ Gerwa well, (location not specified)	Patpara	Mandal (1983) Sharma and Clarke (1982)
140 ± 11	PAT-3/2	OSL (quartz)/ Patpara	Patpara (late Acheulean)	Haslam *et al.* (2011)
137 ± 10	PAT-4/1	OSL (quartz)/ Patpara	Patpara (late Acheulean)	Haslam *et al.* (2011)
58 ± 6	S-1	IRSL (coarse-grained feldspar)/ Sihawal	Patpara	Pal *et al.* (2005) Williams *et al.* (2006)
~100	N-1	IRSL (polymineral fine grains)/ Nakhjar Khurd	Sihawal	Pal *et al.* (2005)
104 ± 20	Alpha 899	TL (polymineral fine grains)/ Nakhjar Khurd	Sihawal	Williams and Clarke (1995) Clark and Williams (1987)
131 ± 10	BAM-1/1	OSL (quartz)/ Bamburi	Sihawal (late Acheulean)	Haslam *et al.* (2011)
125 ± 13	BAM-2/1	OSL (quartz)/ Bamburi	Sihawal (late Acheulean)	Haslam *et al.* (2011)
131 ± 9	BAM-3/2	OSL (quartz)/ Bamburi	Sihawal (late Acheulean)	Haslam *et al.* (2011)

[1]Calibrated radiocarbon ages are from Williams *et al.* (2006) and are expressed at the 95% confidence interval.

Table 3. D_e values, fading rates, OD values and calculated IRSL age estimates for all samples.

IRSL sample #	Sample location (elevation in m asl)	D_e (CAM)[1] (Gy)	n	Average Recycling Ratio	Average Recup. (%)	Uncorrected CAM[1] age (ka)	*g*-value (%/decade)	OD[2] (%)	Fading-corrected CAM[1] age estimate (ka)[2]	Fading-corrected MAM[1] age estimate (ka)[2]
H-1	highest terrace (~27)	48.2 ± 1.0	24	1.01 ± 0.03	2.0 ± 0.1	12.4 ± 0.4	3.2 ± 0.1	7 ± 2	16.4 ± 0.5	16.4 ± 0.6
M-2	dirt road (~20)	20.5 ± 1.9	24	1.00 ± 0.03	5.0 ± 0.1	7.1 ± 0.7	3.5 ± 0.1	47 ± 7	9.6 ± 1.0	5.9 ± 0.7
L-3	lowest terrace (~10 m)	7.8 ± 1.2	24 (16)	1.00 ± 0.03	8.0 ± 0.3	1.6 ± 0.3	3.6 ± 0.1	79 ± 11 (73 ± 13)	2.1 ± 0.4 (3.1 ± 0.6)	0.7 ± 0.1 (1.1 ± 0.2)
M-4	dirt road (~20 m)	18.9 ± 1.5	24	1.00 ± 0.03	5.0 ± 0.2	7.5 ± 1.6	4.0 ± 0.1	48 ± 7	11.0 ± 1.2	4.7 ± 0.6
H-5	highest terrace (~30 m)	40.5 ± 0.8	24	1.00 ± 0.03	2.0 ± 0.1	12.0 ± 0.4	3.6 ± 0.1	5 ± 2	16.7 ± 0.6	16.7 ± 0.7
M-6	dirt road (~20 m)	28.8 ± 2.7	24	1.00 ± 0.03	4.0 ± 0.1	11.3 ± 1.3	3.6 ± 0.1	42 ± 7	15.3 ± 1.7	7.8 ± 1.1
L-7	lowest terrace (~10 m)	11.2 ± 0.9	24 (23)	1.00 ± 0.03	8.0 ± 0.3	2.8 ± 0.3	3.7 ± 0.1	44 ± 6 (45 ± 7)	3.8 ± 0.4 (3.8 ± 0.4)	2.7 ± 0.2 (2.7 ± 0.2)
GHO-2 (below YTT)	Ghoghara main section	54.6 ± 1.7	24	1.01 ± 0.03	1.18 ± 0.04	22.6 ± 1.0	3.1 ± 0.1	20 ± 4	29.3 ± 1.7	21.3 ± 1.6
GHO-3 (above YTT)	Ghoghara main section	77.7 ± 1.9	24	1.00 ± 0.03	1.28 ± 0.04	25.3 ± 0.9	3.1 ± 0.1	13 ± 2	34.4 ± 1.4	31.2 ± 2.0

[1]Age estimates have been calculated from fading-corrected aliquot ages using the CAM and the MAM. A possible 2% beta source calibration error has been added in quadrature to the D_e error.
[2]The ages in parantheses were calculated after rejecting aliquots with recuperation values greater than 10%. Eight aliquots were rejected from L-3, but only one from L-7.

Table 4. Environmental dose rates for all samples.

		Water (%)[1]		**Dose Rates (Gy/ka)**			
IRSL sample #	**Sample location**	**Field**	**Used**	**Beta**	**Gamma**	**Cosmic**	**Total**[2]
H-1	highest terrace	2.5	5 ± 2	1.54 ± 0.08	1.18 ± 0.04	0.19 ± 0.02	3.91 ± 0.10
M-2	dirt road	3.6	5 ± 2	1.08 ± 0.09	0.65 ± 0.02	0.18 ± 0.02	2.91 ± 0.11
L-3	lowest terrace	4.6	10 ± 2	2.10 ± 0.09	1.51 ± 0.05	0.17 ± 0.02	4.79 ± 0.11
M-4	dirt road	0.8	5 ± 2	0.76 ± 0.08	0.60 ± 0.02	0.19 ± 0.02	2.55 ± 0.10
H-5	highest terrace	8.9	10 ± 2	1.38 ± 0.07	0.90 ± 0.03	0.17 ± 0.02	3.45 ± 0.09
M-6	dirt road	1.6	5 ± 2	0.81 ± 0.16	0.57 ± 0.02	0.18 ± 0.02	2.56 ± 0.17
L-7	lowest terrace	9.1	10 ± 2	1.75 ± 0.15	1.17 ± 0.04	0.18 ± 0.02	4.10 ± 0.16
GHO-2 (below YTT)	Ghoghara main section	0.3	5 ± 2	0.72 ± 0.05	0.61 ± 0.03	0.09 ± 0.01	2.42 ± 0.08
GHO-3 (above YTT)	Ghoghara main section	0.9	5 ± 2	1.05 ± 0.05	0.91 ± 0.05	0.11 ± 0.01	3.07 ± 0.09

[1]Measured water contents are shown as 'field', and long-term averaged water contents are shown as 'used'. Corrections for water content were made by dividing dry dose rates by attenuation factors to obtain wet dose rates. Attenuation factors can be calculated as 1+HWF, where H = 1.50 for the alpha dose rate, 1.25 for the beta dose rate, and 1.14 for the gamma dose rate, W = is the saturation water content (defined as the weight of water divided by the dry weight of sediment), and F is the fraction of saturation corresponding to the assumed average water content over the entire burial period (Zimmerman 1971; Aitken 1998). Uncertainties are assigned to accommodate (at 2σ) the field values and any likely variation in water content since sample deposition.

[2]Total dose rate includes environmental beta, gamma, and cosmic ray dose rates, as well as an internal dose rate of 1.00 ± 0.05 Gy/ka derived from U, Th, ^{40}K, and ^{87}Rb inside the K-feldspar grains.

Supplementary Material

Table 1. IRSL sample site coordinates.

IRSL sample site	Latitude	Longitude	Approximate elevation[1] (m)
H-1	24°29.30’N	82°0.66’E	237
M-2	24°29.43’N	82°0.58’E	227
L-3	24°29.60’N	82°0.74’E	218
M-4	24°29.47’N	82°0.92’E	227
H-5	24°29.37’N	82°1.10’E	240
M-6	24°29.50’N	82°1.07’E	237
L-7	24°29.69’N	82°1.35’E	221
GHO-2	24°30.13’N	82°1.05’E	230
GHO-3	24°30.13’N	82°1.05’E	230

[1]Handheld GPS reported accuracy of approximately ±10 m.

Table 2. SAR protocols for KF aliquots measured using the IRSL signal.

1.	Natural / Regenerative Dose[1]
2.	Preheat (250°C, 10 s)
3.	IRSL (50°C, 100 s) → L_n, L_x
4.	Test dose (11 Gy)
5.	Preheat (250°C, 10 s)
6.	IRSL (50°C, 100 s)….→ T_n, T_x
7.	IRSL bleach (290°C, 40 s)
8.	Return to step 1.

[1]Ln = natural signal, Lx = regenerative dose signal. For D_e estimations, regenerative doses of 46, 68, 91, 114, 0 and 68 Gy were used.

Table 3. Anomalous fading SAR measurement protocol.

1.	Dose (28 Gy)
2.	Preheat (250°C, 10 s)
3.	IRSL (50°C, 100 s) → L_x (prompt)
4.	Test dose (11 Gy)
5.	Preheat (250°C, 10 s)
6.	IRSL (50°C, 100 s) → T_x (prompt)
7.	IRSL bleach (290°C, 40 s)
8.	Dose (28 Gy)
9.	Preheat (250°C, 10 s)
10.	**Delay**
11.	IRSL (50°C, 100 s) → L_x
12.	Test dose (11 Gy)
13.	Preheat (250°C, 10 s)
14.	IRSL (50°C, 100 s) → T_x
15.	IRSL bleach (290°C, 40 s)
16.	Return to step 10 for the remaining delay times.